

# Spatiotemporal Mapping of Ultrafine Particle Fluxes in an Office HVAC System with a Diffusion Charger Sensor Array

Danielle N. Wagner, Nusrat Jung, and Brandon E. Boor\*



Cite This: *ACS EST Air* 2025, 2, 49–63



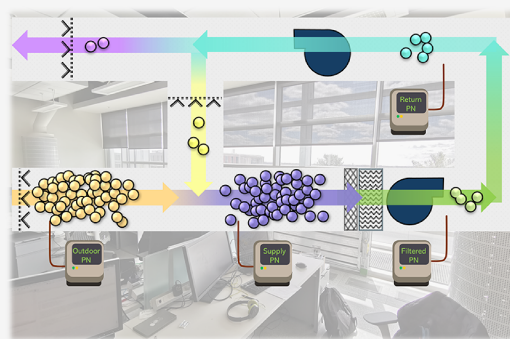
Read Online

ACCESS |

Metrics & More

Article Recommendations

**ABSTRACT:** Commercial HVAC systems intended to mitigate indoor air pollution are operated based on standards that exclude aerosols with smaller diameters, such as ultrafine particles (UFPs,  $D_p \leq 100$  nm), which dominate a large proportion of indoor and outdoor number-based particle size distributions. UFPs generated from occupant activities or infiltrating from the outdoors can be recirculated and accumulate indoors when they are not successfully filtered by an air handling unit. Monitoring UFPs in real occupied environments is vital to understanding these source and mitigation dynamics, but capturing their rapid transience across multiple locations can be challenging due to high-cost instrumentation. This 9-month field measurement campaign pairs four medium-cost diffusion charger sensors with volumetric airflow rates modulated and monitored in a cloud-based building automation system of an open-plan living laboratory office and dedicated air handling unit to evaluate spatiotemporal particle number and surface area concentrations and migration trends. Particle number flux rates reveal that an estimated daily median of  $8 \times 10^{13}$  UFPs enter the air handling unit from the outdoors. Switching from a MERV14 to a HEPA filter reduces the number of UFPs supplied to the room by tens of trillions of UFPs daily, increasing the median filtration efficiency from 40% to 96%. These results demonstrate the efficacy of an optimal air handling unit's performance to improve indoor air quality, while highlighting UFP dynamics that are not accounted for in current filtration standards nor in occupant-centered HVAC control. Scalable sensor development can popularize UFP monitoring and allow for future UFP integration within building control and automation platforms. The framework established for this campaign can be used to evaluate particle fluxes considering different analytes.



**KEYWORDS:** indoor air quality, air pollution sensor network, aerosol dynamics, filtration, ventilation

## INTRODUCTION

Heating, ventilation, and air conditioning (HVAC) systems must be regularly evaluated to ensure that each built environment optimally facilitates occupant well-being and productivity while preventing adverse outcomes from environmental contaminants. Though commercial buildings in the U.S. employ standards such as those defined by the American Society of Heating, Refrigerating, and Air Conditioning Engineers (ASHRAE) to inform safe and efficient building management, emerging and underestimated airborne pollutants can infiltrate and accumulate in workplaces, affecting indoor environmental quality (IEQ). Carbon dioxide ( $\text{CO}_2$ ) is commonly employed as the main bioeffluent for estimating occupancy within demand-controlled ventilation systems; however, it is not always coemitted with aerosols and volatile organic compounds (VOCs) generated from indoor activities, which spurs the need to consider other indoor air quality regulation and exposure thresholds.<sup>1,2</sup> As a widely standardized aerosol exposure metric,  $\text{PM}_{2.5}$ —the size-integrated mass concentration of particles with diameters ( $D_p$ )  $\leq 2,500$

nm—is a strong indicator of fine (100 to 2,500 nm) particles due to their contributions to mass.<sup>3,4</sup> Dynamics of smaller, more numerous ultrafine particles (UFPs,  $D_p \leq 100$  nm), such as those generated from indoor activities,<sup>5</sup> can be understated when using a mass-based metric,<sup>6–8</sup> thus, it is often useful to represent them using particle number (PN) or particle surface area (PSA) concentrations. Indoor and outdoor number-based size distributions are largely dominated by particles ranging from  $\sim 1$  to 300 nm,<sup>3,9–13</sup> while mass-weighted size distributions are dominated by larger diameters ranging from 100 to 10,000 nm.<sup>3,9,10,13</sup>

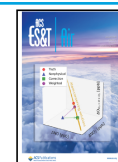
UFPs can be directly emitted into the air, via nanomaterial manufacturing<sup>14</sup> and combustion,<sup>15</sup> or form as secondary

**Received:** June 14, 2024

**Revised:** September 24, 2024

**Accepted:** September 25, 2024

**Published:** December 17, 2024



organic aerosol from precursor reactants. Building occupants induce UFP-generating reactions passively via ozonolysis of skin oil<sup>16</sup> and personal care products,<sup>17</sup> or actively while cleaning,<sup>15,18–20</sup> or using electronics such as drills and laser and 3D printers.<sup>15,21–25</sup> UFP emissions from laser and 3D printers are a prime example of emerging UFP pollutants in both commercial and residential environments that illustrate the importance of real-time monitoring in occupied spaces. Though occupant-specific exposure will vary based on source frequency, proximity, and room conditions, fine and ultrafine aerosols ranging from 10 to 1,000 nm have been shown to exceed PN concentrations of 90,000 #/cm<sup>3</sup> and PSA concentrations of 700  $\mu\text{m}^2/\text{cm}^3$  in offices with 3D printers lacking localized exhaust, greatly exceeding supply air concentrations of PN of 400 #/cm<sup>3</sup> and PSA of 30  $\mu\text{m}^2/\text{cm}^3$ .<sup>25</sup> Emerging evidence of UFP toxicity and intergenerational resilience<sup>26</sup> necessitates exposure prevention by better understanding source emissions and mitigation strategies.

UFP inhalation exposure is associated with high deposition in each region of the respiratory tract, including the head airways, tracheobronchial region, and pulmonary region.<sup>27</sup> The high particle surface area available for adsorption and reactivity<sup>28</sup> enables blood circulation and cellular translocation<sup>29</sup> of UFPs within the body. This has been linked to pulmonary<sup>30</sup> and central nervous system<sup>31</sup> inflammatory responses, metabolic alteration,<sup>32</sup> and cardiovascular stress.<sup>32,33</sup> UFP exposure is also associated with a decline in cognitive performance, including adverse effects on working memory recall and motivation,<sup>34,35</sup> notably in schoolchildren and adults shown to be susceptible to Alzheimer's.<sup>36,37</sup> Because of this linkage, PSA and lung-deposited surface area concentrations have been suggested as effective metrics for UFP toxicity exposure<sup>38,39</sup> and even as building control metrics.<sup>25</sup>

Despite recent stricter global air quality limits<sup>40</sup> and the growing body of evidence toward UFP toxicity,<sup>29,41</sup> exposure limits that adequately reflect UFP levels, such as number or surface area metrics, remain sparse. The World Health Organization recently issued "good practice statements" for UFPs while updating air quality guidelines for other pollutants, citing a daily ambient mean PN of less than 1,000 UFP/cm<sup>3</sup> as "low" based on low-anthropogenic emission environments, and 20,000 UFP/cm<sup>3</sup> (1-h mean) or 10,000 UFP/cm<sup>3</sup> (24-h mean) as "high", based on urban levels.<sup>40</sup> Nanomaterial exposure limits have been adopted in more specific contexts,<sup>42</sup> including 40,000 UFP/cm<sup>3</sup> as an 8-h nanomaterial exposure standard.<sup>43</sup>

Building automation systems provide an interactive interface to modulate control-based setpoints based on IEQ parameters and monitor real-time environmental dynamics to inform operations. Because buildings act as sources and sinks for atmospheric pollutants,<sup>44</sup> monitoring is also essential to consider the environmental exchange between the indoors and outdoors for reaching zero-emission efficiency goals.<sup>45</sup> Commercial HVAC systems ensure that the air handling unit effectively supplies low concentrations of CO<sub>2</sub> through ventilation and low aerosol concentrations via filtration, following ASHRAE 62.1-2022 (Ventilation and Acceptable Indoor Air Quality) and 52.2-2017 (Method of Testing General Ventilation Air-Cleaning Devices for Removal Efficiency by Particle Size), respectively.<sup>46,47</sup> The most updated minimum efficiency reporting value (MERV) for filters as outlined in ASHRAE 52.2 is defined for particles ranging 300 to 10,000 nm, which excludes UFPs and thus the

majority of particles dominating indoor number size distributions.<sup>46</sup> Size-resolved filtration efficiencies estimated for commonly used filters have revealed large variations in particle removal depending on particle size.<sup>13</sup> UFP loading has been shown to increase filtration efficiencies by varying amounts based on composition, explained by phenomena such as when dendritic chains form on electrostatic filters to create higher potential for contact with incoming aerosols.<sup>48</sup> Median efficiencies for UFP removal estimated for MERV12 filters were highly variable, ranging from 30% to 80%, depending on the brand.<sup>13,49</sup> Chamber-based filter testing can also overestimate in situ filter efficiency<sup>50</sup> when not reflecting variable airflow rates<sup>51</sup> and realistic aerosol profiles. Lower-rated MERV filters sometimes outperform those that are more highly rated for certain size ranges.<sup>13</sup> These measurement and rating discrepancies highlight the importance of including metrics encompassing smaller particles, such as PN and PSA concentrations, within building standards, as well as monitoring them in real occupied environments in order to ensure the capacity of HVAC systems to adequately mitigate nano-sized aerosols.

Integrating air quality sensors and networks within building automation systems would expand HVAC control to aerosols in addition to CO<sub>2</sub>;<sup>52</sup> however, barriers remain toward achieving scalable, accurate measurement systems encompassing transient UFP dynamics.<sup>53,54</sup> High-end instrumentation can be used to collect high-resolution temporal particle size distributions accounting for smaller diameters but can be challenging to obtain spatially resolved distributions due to lack of portability and high up-front costs. Automated valve-switching allows for proximal upstream-downstream measurements at alternating times, such as at indoor-outdoor nodes,<sup>11,55</sup> supply and return air,<sup>56</sup> and pre- and postfilter for reporting filtration efficiencies.<sup>57–59</sup> Manually relocating instruments or sample tubing can also be used to gather short-term outdoor concentrations.<sup>60,61</sup> Spatiotemporal low-cost commercialized or microcontroller-based optical particle counter sensor fleets operating on light scattering principles have been used to visualize larger, coarse mode particle drift from source emissions<sup>62–66</sup> but do not effectively capture particles below 300 nm due to their decreased refractive abilities at smaller sizes.<sup>67,68</sup>

Portable, medium-cost (~\$10,000 USD) aerosol instrumentation offers a more affordable way to measure total size-integrated concentrations of fine and ultrafine particle metrics, including PN, PSA, and lung-deposited surface area. Hand-held condensation particle counters condense the vapors of a working fluid onto smaller particles to enable their detection by an internal optical particle counter,<sup>69</sup> with high detection efficiencies up to PN concentrations of 10<sup>5</sup> UFP/cm<sup>3</sup> for particles down to around 10 nm.<sup>70,71</sup> These condensation particle counters have been used in offices for dynamic comparisons of the indoor-outdoor air in smoking environments<sup>61</sup> and across multiple countries,<sup>72</sup> offering insight into their portability and rigor. Portable unipolar diffusion charger sensors ionize an aerosol sampling stream that creates a current detected by an internal electrometer, first correlating the charge to PSA. This design protects the corona needle without the use of a fluid, resulting in even higher detection limits (PN concentrations up to 10<sup>7</sup> UFP/cm<sup>3</sup>) for particles that may range in size from around 10 to 2,500 nm, depending on the specific sensor, allowing them to be left unattended in high concentration environments during passive sampling.<sup>60,73,74</sup>

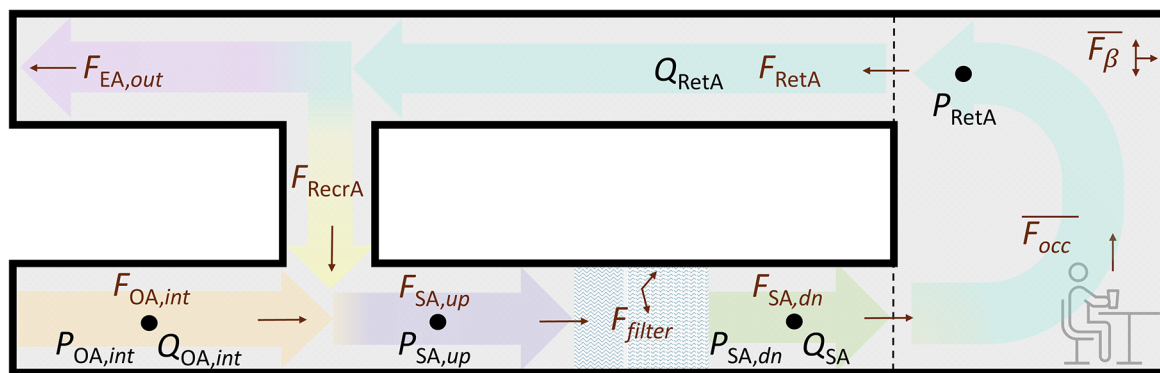


**Figure 1.** Open-plan office HVAC schematic. Number-based UFP fluxes ( $F_{node}$ ) were estimated at the outdoor air intake, supply air upstream and downstream of the HVAC filter bank, return air, exhaust air, and recirculation air locations in the air handling unit. Time-averaged occupant-sourced UFP fluxes and UFP deposition fluxes were estimated within the office room itself. Nodes ( $P_{node}$ ) indicate each of the four diffusion charger sampling locations. Volumetric airflow rates ( $Q_{node}$ ) were measured as part of the office building automation system platform.

Hand-held unipolar diffusion chargers (DiSCmini, Testo, Titisee-Neustadt, Germany) have been used to temporally compare PN concentrations ( $10 \text{ nm} \leq D_p \leq 300 \text{ nm}$ ) in multiple rooms in an academic building to hallway and outdoor concentrations.<sup>54</sup> Viitanen et al. measured fine and ultrafine particles in a single office at a 3D printer, workstation, and the supply and return air vents utilizing four Pegasor AQ Indoor diffusion charger sensors (Pegasor Oy, Tampere, Finland).<sup>25</sup> Measured concentrations were used to model source emission and loss rates among varying ventilation control methods. These lower-cost options facilitate spatio-temporal sampling that can capture rapid UFP dynamics across a single room or multiple rooms, limiting differences in sampling variability.

To the best of the authors' knowledge, there are no existing studies using diffusion charger sensors to simultaneously measure total particle number and surface area concentrations at multiple points in an occupied open-plan office and dedicated air handling unit, leaving a gap in understanding UFP rapid migration and transformation dynamics throughout an HVAC system. This work takes advantage of four Pegasor AQ Indoor diffusion chargers and a cloud-based building automation system platform with Java Application Control Engine (JACE) control (Niagara Framework, Tridium Inc., Richmond, Virginia, U.S.) to explore spatiotemporal UFP dynamics in the HVAC system of a living laboratory situated in a Leadership in Energy and Environmental Design (LEED)-Gold high-performance building over the course of 9 months. Measurements were made simultaneously at four locations (Figure 1): directly in an occupied open-plane office, at the outdoor air intake, at the mixed supply air upstream of an air handling unit filter bank, and at the supply air downstream of the filter. A long-term campaign and assessment framework based on a simplified material balance model is established to integrate simultaneous multinodal aerosol monitoring paired with online volumetric airflow measurements. Spatiotemporal UFP dynamics are evaluated at each stage in the HVAC system (Figure 1) using monitored PN and PSA concentrations and number-based flux rates to illustrate migration, as well as the HVAC system's capacity to mitigate UFPs sourced from occupant activities and the outdoors. Suggested future work may include integrating portable diffusion charger sensor

informatics within a building automation system to enable UFP-based sensing and control within HVAC systems.

## MATERIALS AND METHODS

**Study Site: Open-Plan Living Laboratory Office and Dedicated Air Handling Unit.** The long-term monitoring campaign was carried out at the Ray W. Herrick Laboratories, a high-performance LEED-Gold Certified building located in the southwestern area of Purdue University's West Lafayette campus, situated within a mile radius of a major highway and several main roads, a small airport, and a natural gas and coal power plant. Each of the four open-plan living laboratories on the third floor operates with a dedicated mechanical room and HVAC system, allowing for isolated control scenario modulation for IEQ and utility efficiency testing.<sup>75,76</sup> The full sampling campaign spanned 9 months, from mid-February to mid-November in 2019, with several gaps in data due to power outages and unforeseen technical issues. Of the four open-plan living laboratories, the office that was selected for this sampling campaign was chosen due to consistently achieving the highest occupancies, often reaching 6 people at a time, and peaking at 12 people (maximum occupancy of 20 people).<sup>77</sup> While each living laboratory has unique methods of air delivery, the chosen office includes options for supply air delivery through floor vents, natural ventilation double-skin façade openings, and wall diffusers. The online Niagara framework with JACE control was used for real-time monitoring and offline data acquisition of HVAC parameters, including heating coil temperatures, air temperatures, relative humidities, fan speeds, and airflow rates.

The HVAC system was configured as a variable air volume system with air delivered mainly via equally spaced floor vents throughout the campaign, where heating and cooling coil temperatures remain constant, and airflow rates are varied to maintain adequate ventilation. Thus, damper positions (% open or closed) and supply and return fan speeds were adjusted to achieve various room pressurizations and air delivery scenarios. The filter bank in the air handling unit included a prefilter (MERV8) and main filter, where a MERV14 was used from mid-February to mid-May (99 days, 42% of campaign) and changed to a HEPA filter from mid-May to mid-November (138 days, 58% of campaign). Additional aspects regarding instrumentation and configura-

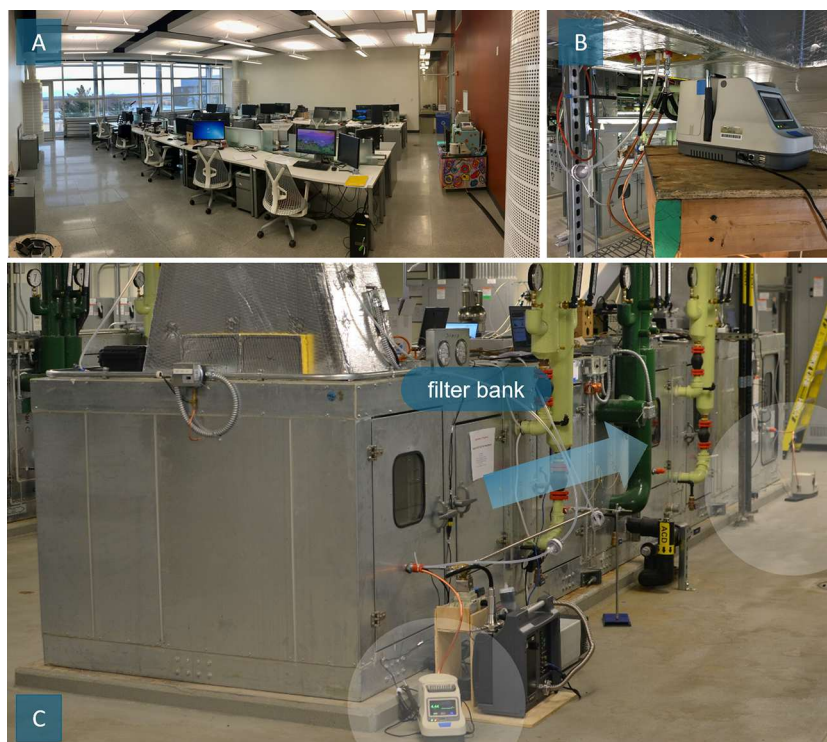


**Figure 2.** UFP monitoring for the office and its air handling unit with a diffusion charger sensor array. (a) Room air diffusion charger sampling location in the living laboratory office. (b) Outdoor air intake diffusion charger sampling location. (c) Diffusion charger sampling locations for the supply air upstream and downstream of the HVAC filter bank. An arrow is included to show the airflow direction for the supply air through the air handling unit.

tions pertaining to this living laboratory campaign can be found in studies that detail the ventilation mode and influence of variable air volume control,<sup>78</sup> seated occupancy measurements,<sup>77</sup> and indoor air measurements including VOCs,<sup>44</sup> ozone,<sup>58</sup> CO<sub>2</sub>,<sup>78</sup> and fluorescent aerosol particles.<sup>79</sup> High-resolution spatiotemporal and total office occupancy was approximated during the campaign using chair-embedded K-type thermocouples to estimate seated occupancy, enabling pairing with airborne emissions in each subsequent study.

**Aerosol Instrumentation: UFP Monitoring with a Diffusion Charger Sensor Array.** Four Pegasor AQ Indoor diffusion charger sensors were used to simultaneously measure fine and ultrafine ( $10 \text{ nm} \leq D_p \leq 2,500 \text{ nm}$ ) number and surface area concentrations (1 Hz) at four different nodes in the living laboratory HVAC system ( $P_{\text{node}}$ , Figure 1): directly in the office; in the outdoor air duct; in the supply air upstream of the filter bank that includes a combination of recirculated return air and outdoor air; and a second supply air location downstream of the filter bank, which is delivered to the office. The outdoor air node was measured from mid-July to mid-September, while the other three were in-place during the full campaign (February to November). To measure in each of the three air handling unit duct locations, 1 m of 12.7 mm-diameter conductive copper tubing was connected to the inlet of each diffusion charger sensor, led to a pre-existing duct opening, and fastened with a silicone cap to minimize leakage (Figure 2). Measured number and surface area concentrations were corrected for accuracy using a calibration previously described in Wagner et al.<sup>60</sup> by comparing simultaneous diffusion charger measurements of size-selected NaCl and KCl particles<sup>80</sup> to a water-based condensation particle counter (wCPC, Model 3788, TSI Inc., Shoreview, MN, U.S.), as well

as corrected for precision with a collocation of four Pegasor sensors monitoring laboratory-generated woodsmoke in a chamber.<sup>60</sup>

**Representing Transient UFP Dynamics in an HVAC System: Estimation of UFP Flux Rates.** The diagram and temporal plots in Figure 3 are included to represent measured particle number concentrations (Figure 3b), volumetric airflow rates (Figure 3c), and room occupancy (Figure 3d) of a select day with distinguishable peaks as well as the resulting estimated flux rates (Figure 3e, f) at each node. Figure 3b illustrates the UFP measurements made at each monitored location over the course of a 14 h period of a day, where each location is color-coded to the HVAC schematic (Figure 3a) and to each term in subsequent figures. The term  $P_{\text{node}}$  is used to represent a particle-monitored node and is interchangeable with particle number ( $PN_{\text{node}}$ ) or particle surface area ( $PSA_{\text{node}}$ ) concentrations. While number-based size distributions often include contributions from particles as large as 300 nm, the PN and PSA concentrations monitored in this study will be referred to as UFPs due to the majority of particles represented in these distributions being 100 nm or less.<sup>9–12</sup> In a previous study for this campaign over the course of a select day with over 50% recirculation, the particles in the supply air were represented by 90% ultrafine (6 to 100 nm), 0.09% for 100 to 300 nm, and 0.01% for 300 to 2,500 nm as determined by measurements with a High-Resolution Electrical Low Pressure Impactor (HR-ELPI+, Dekati Ltd., Tampere, Finland).<sup>58</sup> In a comparison of deposition proportions in-room vs ventilation systems, Nazaroff and Sippola estimated that duct loss for sub-micron particles is minimal compared to active filtration loss.<sup>81</sup> The office room UFP concentrations ( $P_{\text{RmA}}$ ) are thus assumed to be the same as those in the nodes at the

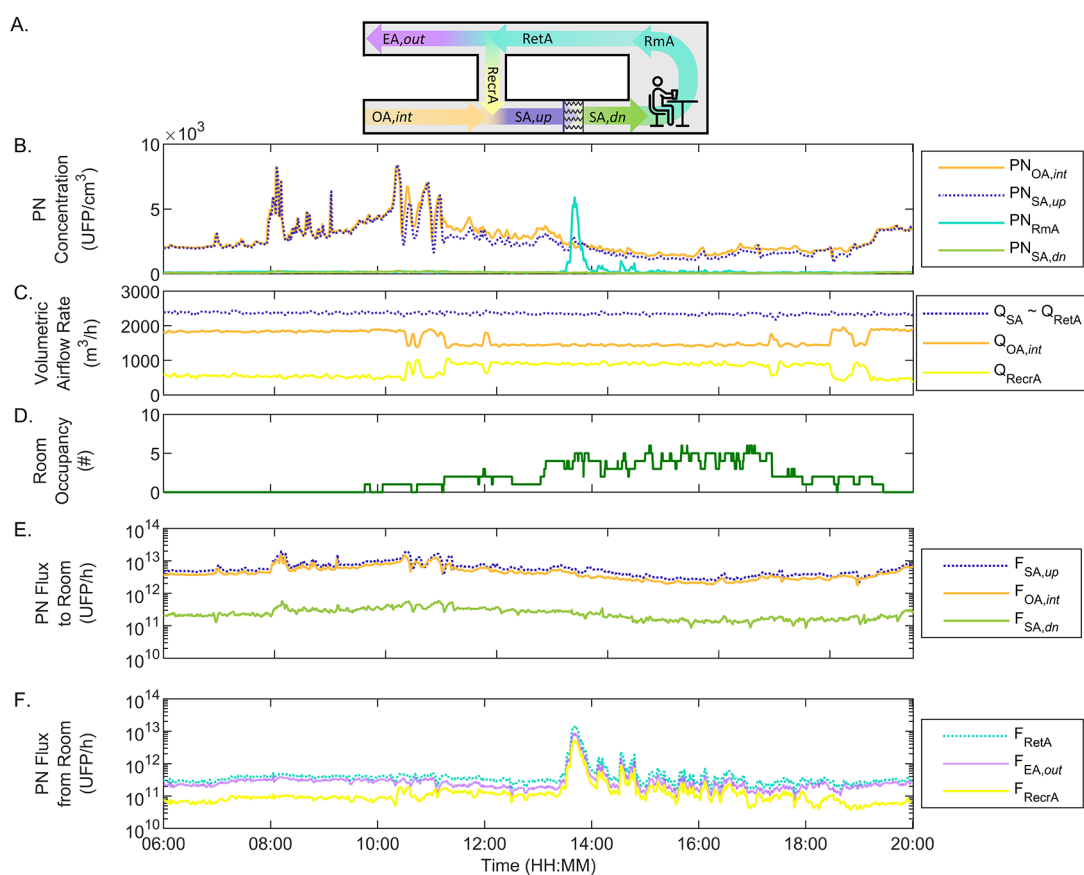


**Figure 3.** Temporal composite plots for a select day of measurement delineating the UFP number concentration and volumetric airflow rate measurements enabling spatiotemporal UFP flux rate estimations in an occupied office over the course of a 14-h period, selected to highlight diurnal variations, throughout which a HEPA filter was used. (a) Simplified schematic denoting the direction of airflow throughout the HVAC system, color-coded based on outdoor air ( $OA_{,int}$ ; orange), supply air upstream ( $SA_{,up}$ ; purple) and downstream ( $SA_{,dn}$ ; lime green) of the HVAC filter bank, room and return air ( $RmA$ ,  $RetA$ ; teal), exhaust air ( $EA_{,out}$ ; magenta), and recirculation air ( $RecrA$ ; yellow). (b) UFP total number concentrations measured at each of the 4 locations using diffusion charger sensors. (c) Volumetric airflow rates monitored using the building automation system platform. (d) Seated room occupancy within the office representing total occupancy.<sup>77</sup> UFP PN flux estimated (e) upstream and (f) downstream of the office space.

return ( $P_{RetA}$ ), exhaust ( $P_{EA,out}$ ), and recirculation ( $P_{RecrA}$ ) due to relatively negligible UFP deposition to HVAC duct surfaces. The other three nodes were located in the air handling unit at the outdoor air intake ( $P_{OA,int}$ ) and supply air upstream ( $P_{SA,up}$ ) and downstream ( $P_{SA,dn}$ ) of the HVAC filter bank.

Volumetric airflow rates ( $Q_{node}$ ) were measured each minute using air velocity mass flow transducers and later downloaded from the Niagara system at the supply fan (supply air,  $Q_{SA}$ ), return fan (return air,  $Q_{RetA}$ ), and outdoor air intake ( $Q_{OA,int}$ ) locations. The return and supply volumetric airflow rates were equated, assuming relatively negligible infiltration and exfiltration across the office room envelope due to the continuously operating HVAC system,<sup>82</sup> thus allowing the outdoor and exhaust ( $Q_{EA,out}$ ) airflow rates to also be equated. The recirculation airflow rate ( $Q_{RecrA}$ ) was estimated as a difference between the return and exhaust airflow rates. Example airflow rates are listed in Figure 3c. Instantaneous spikes in the raw airflow rates resulting from mode shifts were manually removed by identifying weekly outliers that exceeded the majority of the data by 340 m<sup>3</sup>/h.

A flux balance model was developed based on material balance principles for UFP dynamics, where a number-based UFP flux rate ( $F_{node}$ ) is estimated for a specific node and time.

$$F_{node} = PN_{node} \cdot Q_{node} \quad (1)$$

Estimating UFP flux rates (UFP/h) from the number concentrations and airflow rates allows insight into UFP spatiotemporal dynamics within the HVAC system by mapping UFP movement and migration throughout the office and its air handling unit, which are evaluated over time and among different locations. Flux rates for UFP number concentrations were directly estimated using eq 1 for the outdoor air intake ( $F_{OA,int}$ ) and supply air handling unit nodes upstream and downstream of the HVAC filter bank ( $F_{SA,up}$ ,  $F_{SA,dn}$ ). The flux for the return air following the room ( $F_{RetA}$ ) was estimated by equating the return and room air concentrations. The flux rates for the exhaust air ( $F_{EA,out}$ ) and recirculation air ( $F_{RecrA}$ ) were then also indirectly estimated by equating the number concentrations to that in the room air and using the estimated volumetric airflow rates as described previously. Though it is notable that there is likely a non-zero particle loss in the return air duct that could be further estimated through more rigorous chamber studies, the magnitude of the resulting flux rates would be minimally affected by accounting for this loss. Figure 3 illustrates temporal measurements included in the process of estimating UFP flux rates based on the monitored PN concentrations and volumetric airflow rates at each measured and estimated node.

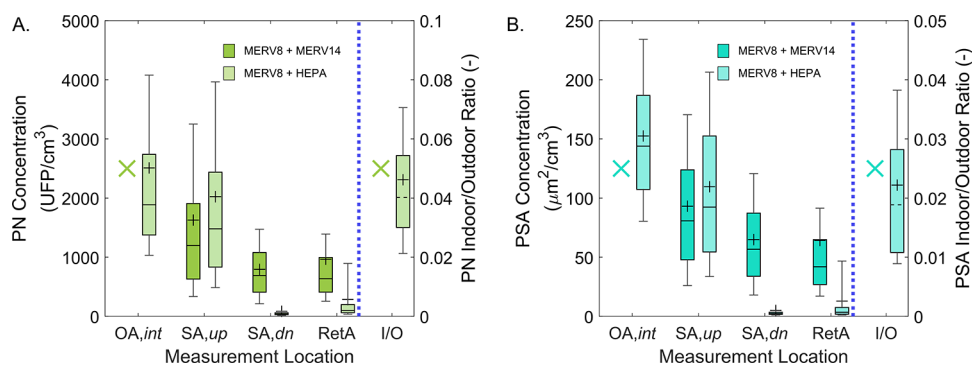


**Figure 4.** UFP total PN and PSA concentrations: mean (+), median (–), 25th and 75th percentiles (boxes), and 10th and 90th percentiles (whiskers), for PN (a) and PSA (b) concentrations are shown from the full campaign measurements at each of the four sampled nodes, including outdoor air intake, supply air upstream and downstream of the HVAC filter bank, and office return air. The measurements are divided based on the filter type used at the time. There were no outdoor air measurements while the MERV14 filter was in place (indicated by an 'X'), thus the indoor/outdoor ratio based on the indoor (return) and outdoor measurements is only included for the HEPA period.

**Table 1. Median Particle Number and Surface Area Concentrations Measured at Each Location<sup>a</sup>**

Location	MERV14 (if applicable); HEPA					
	Particle Number (UFP/cm <sup>3</sup> )			Particle Surface Area (μm <sup>2</sup> /cm <sup>3</sup> )		
	Median	25th percentile	75th percentile	Median	25th percentile	75th percentile
Outdoor Air	$1.9 \times 10^3$	$1.3 \times 10^3$	$2.7 \times 10^3$	<b>140</b>	<b>110</b>	<b>190</b>
Supply Air, Up	<i>1.2 × 10<sup>3</sup></i>	<i>630</i>	<i>1.9 × 10<sup>3</sup></i>	<i>80</i>	<i>50</i>	<i>120</i>
	<b>1.5 × 10<sup>3</sup></b>	<b>830</b>	<b>2.4 × 10<sup>3</sup></b>	<b>90</b>	<b>50</b>	<b>150</b>
Supply Air, Down	<i>690</i>	<i>410</i>	<i>1.0 × 10<sup>3</sup></i>	<i>60</i>	<i>30</i>	<i>90</i>
	<b>40</b>	<b>30</b>	<b>60</b>	<b>2.5</b>	<b>1.7</b>	<b>3.5</b>
Room Air	<i>640</i>	<i>410</i>	<i>990</i>	<i>40</i>	<i>30</i>	<i>60</i>
	<b>100</b>	<b>60</b>	<b>200</b>	<b>3</b>	<b>2</b>	<b>8</b>

<sup>a</sup>Italic numbers are MERV14. Bold numbers are HEPA.

UFP loss was quantified across the HVAC filter bank using the measured size-integrated UFP concentrations in the upstream and downstream supply air to elucidate filter efficiency ( $\eta_{\text{filter}}$ , %).

$$\eta_{\text{filter}}(\%) = \frac{PN_{SA,up} - PN_{SA,dn}}{PN_{SA,up}} \cdot 100\% \quad (2)$$

The filter UFP loss flux ( $F_{\text{filter}}$ ) was then estimated as a differential, which can be conceptualized as a UFP air exchange rate, where a proportion of the office air volume is replenished over a given period of time.

$$F_{\text{filter}} = (PN_{SA,up} - PN_{SA,dn}) \cdot Q_{SA} = F_{SA,up} - F_{SA,dn} = \Delta F_{SA} \quad (3)$$

By assuming negligible infiltration and exfiltration across the office room envelope, the main UFP loss processes in the room include deposition to interior office surfaces ( $F_{\beta}$ ) and return air removal ( $F_{\text{RetA}}$ ). For the scope of estimating UFP fluxes for the office room, coagulation is considered to play a minor role as PN concentrations were generally low in the room ( $\leq 1,000$  UFP/cm<sup>3</sup>). Thus, the total UFP loss flux for the room is the sum of  $F_{\beta}$  and  $F_{\text{RetA}}$ . Office room sources are understood to be those generated by occupants ( $F_{\text{occ}}$ ) and brought in through the supply air ( $F_{SA,dn}$ ). Thus, the total UFP source flux for the room is the sum of  $F_{\text{occ}}$  and  $F_{SA,dn}$ .

Toward estimating a UFP deposition flux to interior office surfaces, a room-based first-order size-integrated deposition loss rate coefficient ( $\beta_{\text{Rm}}$ ) (1/h) was first estimated during steady-state periods over hourly increments to account for changes in supply and return volumetric airflow rates. An office room volume ( $V$ ) of 333 m<sup>3</sup> was used.

$$\beta_{\text{Rm}} \cong \frac{Q_{SA}}{V} \left( \frac{PN_{SA,dn} - PN_{\text{RetA}}}{PN_{\text{RetA}}} \right) = \frac{F_{SA,dn} - F_{\text{RetA}}}{V \cdot PN_{\text{RetA}}} \quad (4)$$

In order to eliminate extraneous source or removal processes occurring during occupied periods,  $\beta_{\text{Rm}}$  was estimated only during vacant, late-night hours (12 AM–6 AM), when the difference of the supply and return airflow rates exceeded 170 m<sup>3</sup>/h, and room PN concentrations exceeded a background of 300 UFP/cm<sup>3</sup>. Using this process, the median and mean deposition loss rate coefficients of the room during unoccupied periods were estimated to be 0.479 and 0.725 1/h, respectively. Though deposition is highly size dependent, these coefficients were deemed reasonable due to falling within the range estimated for particles smaller than 100 nm, which have been shown to be in the range of 0.1 to 1 1/h, as well as a previously estimated size-integrated deposition loss rate coefficient for fine particles of 0.39 1/h.<sup>83,84</sup> The median coefficient was then used as a static term to estimate hourly UFP deposition fluxes in the office room ( $\overline{F_{\beta}}$ ), representing collective UFPs

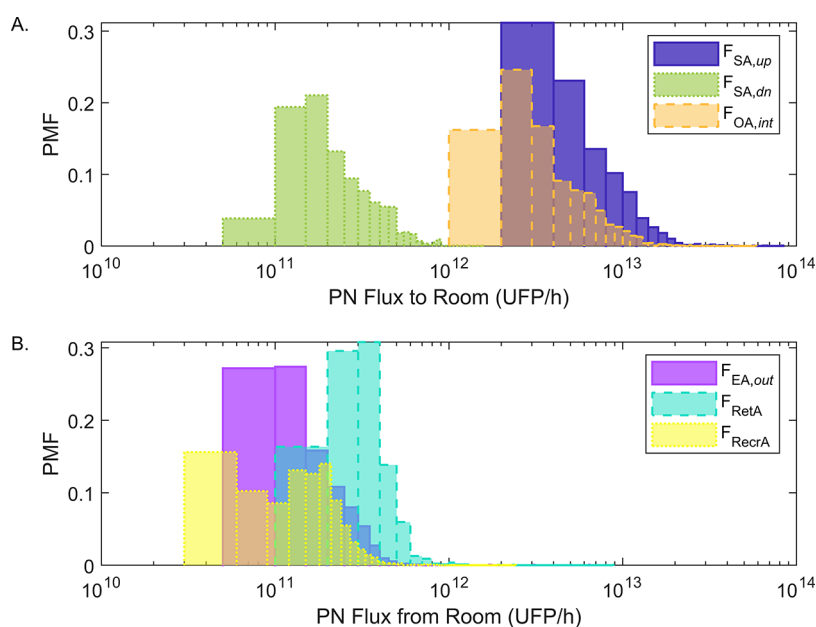


**Figure 5.** Probability mass functions (PMF) illustrating spatiotemporal UFP number flux rates (UFP/h) at each location in an office and its air handling unit. (a) Upstream of the office: outdoor air, prefilter supply air, and postfilter supply air. (b) Downstream of the office: return air, exhaust air, and recirculation air.

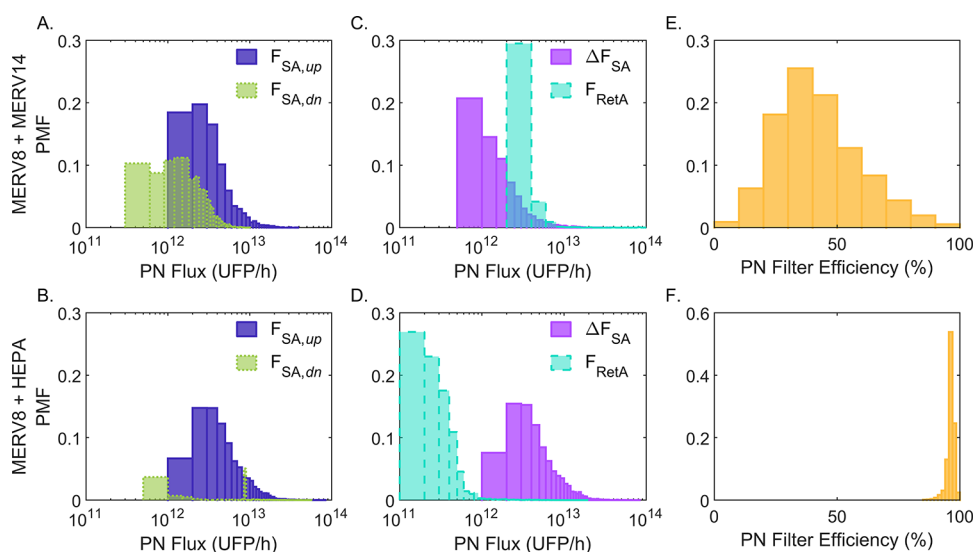


**Figure 6.** (a, b) Probability mass functions (PMFs) of estimated UFP fluxes upstream and downstream of (a) MERV8 prefilter + MERV14 filter (99 days; February to May) and (b) MERV8 prefilter + HEPA filter (178 days; May to November). (c, d) The differential between the UFP fluxes upstream and downstream of the HVAC filter bank ( $\Delta F_{SA}$ , eq 3), illustrating the effect of the filters on UFP loss, as compared to the UFP PN flux in the return air. (e) Efficiency (eq 2) of the MERV8 prefilter + MERV14 filter and (f) the MERV8 prefilter + HEPA filter.

depositing via Brownian and turbulent diffusion over the course of an hour.

$$\overline{F_{\beta}} \cong \overline{\beta_{Rm} PN_{RetA}} V \quad (5)$$

Occupant-sourced UFP fluxes were then estimated over 30-minute increments ( $\overline{F_{occ}}$ ).

$$\overline{F_{occ}} \cong \overline{F_{RetA}} - \overline{F_{SA,dn}} + \overline{F_{\beta}} \quad (6)$$

When distinguished as known high-concentration events, each estimated occupant-sourced UFP flux can be understood as an indoor-associated UFP emission rate.

## RESULTS AND DISCUSSION

**Spatiotemporal Dynamics of UFPs in an Office HVAC System.** The use of four diffusion chargers enabled simultaneous multinodal UFP measurements to explore highly transient UFP dynamics in the room and its air handling unit. Figure 4 summarizes the UFP total PN and PSA concentrations measured at each of the nodes, sorted into a MERV14 or HEPA period. Median concentrations for each of these locations are shown in Table 1, separated into filtration periods when available. The UFP fluxes estimated in this campaign represent the size-integrated particle migration and removal rates on a number basis, allowing insight into concentration

magnitudes at varying airflow rates, capturing generation and movement within and across nodes.

Figure 5 represents the probability mass function (PMF) of the UFP fluxes estimated at each location associated with the office and its air handling unit for the full sampling campaign, where each set of histograms illustrates the proportion (y-axis) of flux at each value (x-axis), summing to 1, and is further broken down by MERV14 or HEPA periods in Figures 6 and 7. The order of highest to lowest median flux rates while all

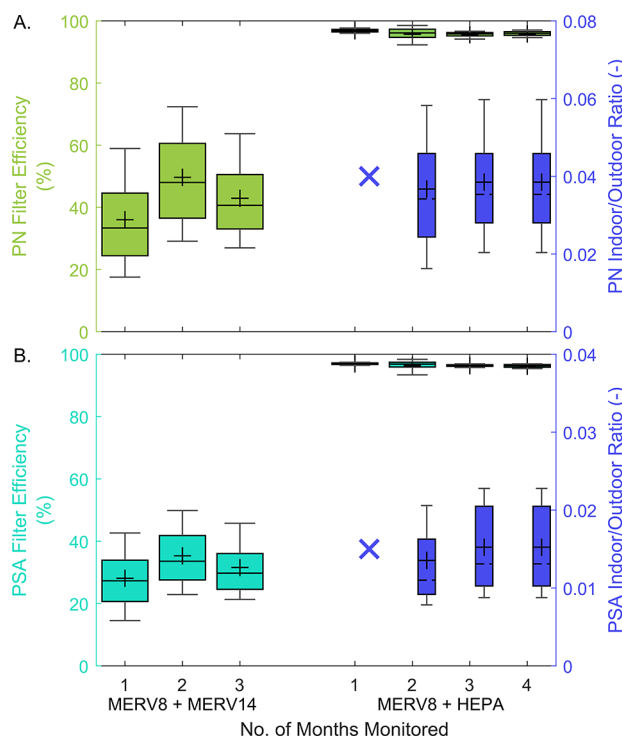


**Figure 7.** Filter efficiencies over time during the period of monitoring for (a) PN (green) and (b) PSA (teal), compared to I/O ratios during the HEPA period (blue, right). The MERV14 filter had already been in use before the campaign, and the HEPA was newly installed. X's indicate missing PN and PSA outdoor data.

sensors were present within the HVAC system is *upstream supply air > outdoor air intake*  $\gg$  *return air > downstream supply air > recirculation air > exhaust air*. Median flux values are shown along with the 25th and 75th percentiles in Table 2. The relative UFP flux rates estimated in this study also align with a similar finding by Jiang et al., where the magnitudes of the air handling unit UFP delivery are discernably less than rapid in-room emission rates identified by specific sources.<sup>4</sup> Elucidated occupant-sourced emission rates from 30 known events are illustrated in Figure 8; the concentrations and resulting fluxes for three singular known emission sources are represented temporally in Figure 9. In addition to providing insight into air handling unit performance and mitigation dynamics, the UFP flux at different locations can be used to roughly estimate the total particles passing through each location by multiplying the flux rate (UFP/h) by a time scale and proportionately scaling the result to different time units (e.g., daily UFP = UFP/h  $\cdot$  24 h/day). Figure 10 displays the estimated number-based magnitudes of UFPs entering and leaving the building for the monitored office air handling unit at various time scales, proportionately based on the estimated median hourly UFP flux for the outdoor air intake and exhaust

**Table 2. Median Particle Number Flux Rates at Each Location<sup>a</sup>**

Location	MERV14 (if applicable); HEPA		
	Particle Number Flux (UFP/h)		
	Median	25th percentile	75th percentile
Outdoor Air	$3.5 \times 10^{12}$	$2.3 \times 10^{12}$	$6.0 \times 10^{12}$
Supply Air, Up	<i><math>2.9 \times 10^{12}</math></i> <b><math>4.1 \times 10^{12}</math></b>	<i><math>1.5 \times 10^{12}</math></i> <b><math>2.3 \times 10^{12}</math></b>	<i><math>4.6 \times 10^{12}</math></i> <b><math>7.1 \times 10^{12}</math></b>
Supply Air, Down	<i><math>1.7 \times 10^{12}</math></i> <b><math>1.7 \times 10^{11}</math></b>	<i><math>9.8 \times 10^{11}</math></i> <b><math>1.1 \times 10^{11}</math></b>	<i><math>2.6 \times 10^{12}</math></i> <b><math>3.1 \times 10^{11}</math></b>
Return Air	<i><math>1.5 \times 10^{12}</math></i> <b><math>2.6 \times 10^{11}</math></b>	<i><math>9.9 \times 10^{11}</math></i> <b><math>1.6 \times 10^{11}</math></b>	<i><math>2.4 \times 10^{12}</math></i> <b><math>3.8 \times 10^{11}</math></b>
Exhaust Air	<i><math>4.7 \times 10^{11}</math></i> <b><math>1.1 \times 10^{11}</math></b>	<i><math>1.0 \times 10^{11}</math></i> <b><math>6.3 \times 10^{10}</math></b>	<i><math>1.4 \times 10^{12}</math></i> <b><math>1.9 \times 10^{11}</math></b>
Recirculation Air	<i><math>7.4 \times 10^{11}</math></i> <b><math>1.2 \times 10^{11}</math></b>	<i><math>2.3 \times 10^{11}</math></i> <b><math>6.0 \times 10^{10}</math></b>	<i><math>1.3 \times 10^{12}</math></i> <b><math>2.0 \times 10^{11}</math></b>

<sup>a</sup>Italic numbers are MERV14. Bold numbers are HEPA.

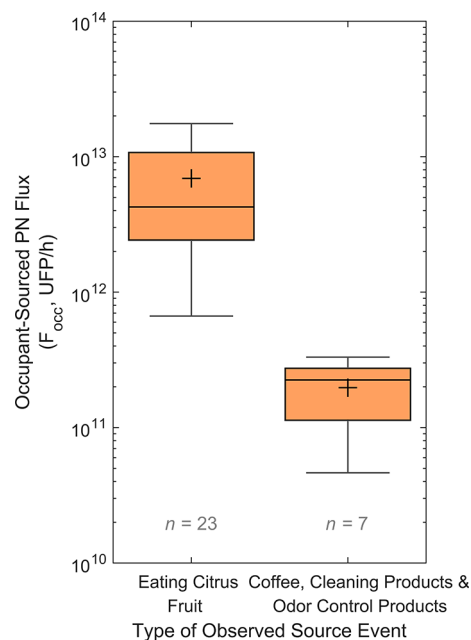


**Figure 8.** Occupant-sourced UFP flux rates, analogous to source emission rates, estimated for 30 observed occupant activities within the office room (eq 6).

air. The following sections refer to the total PN and PSA concentrations (Figure 4), estimated flux values (Figures 5, 6, and 7), temporal trends (Figures 3 and 8), and time-integrated total UFPs (Figure 10) to discuss UFP dynamics within and between each of the major nodes in the HVAC system (Figure 1).

**Outdoor Air.** Outdoor air UFP concentrations were measured over the course of 2 months in the summer (July to September), with a median  $PN_{OA,int}$  of  $1.9 \times 10^3$  UFP/cm<sup>3</sup>. Out of 64 sampling days, 32 days reached or exceeded a PN of  $1 \times 10^4$  UFP/cm<sup>3</sup>, which occurred at various times throughout the day and different days of the week. A long-term study

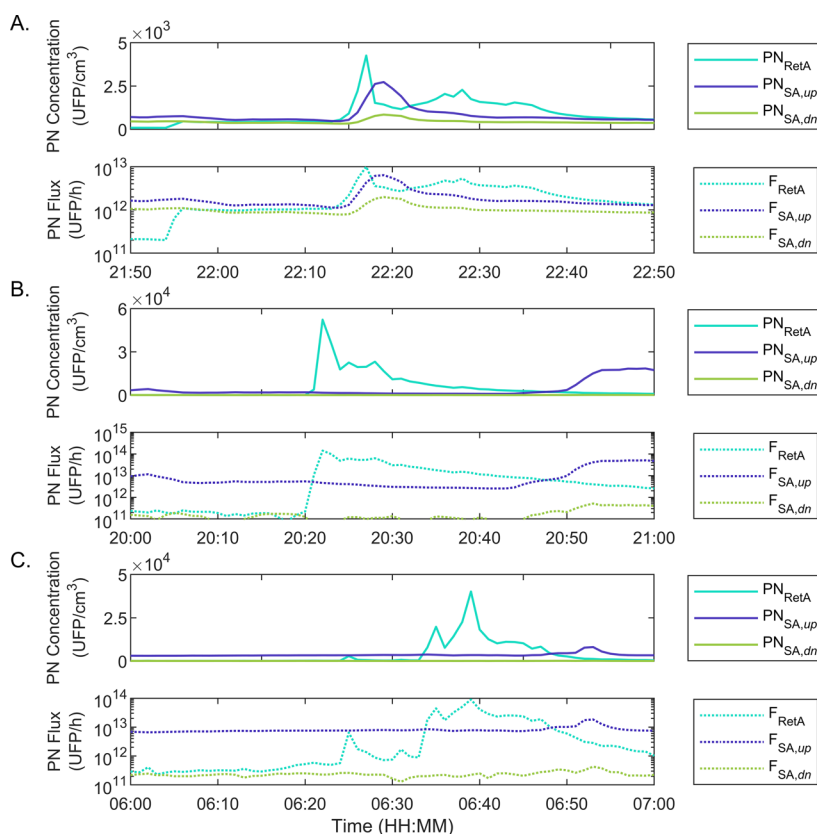


**Figure 9.** Temporal number plots for 3 singular emission events illustrating the monitored UFP PN concentrations and estimated UFP number flux rates at the return air and upstream and downstream supply air nodes, among select source events: (a) Using an oil diffuser (2/16, 21:54) followed by peeling a mandarin (22:12). (b) Peeling and consuming a mandarin (5/31, 20:17). (c) Cleaning the office floor via dusting and burnishing (6/14, 6:24).

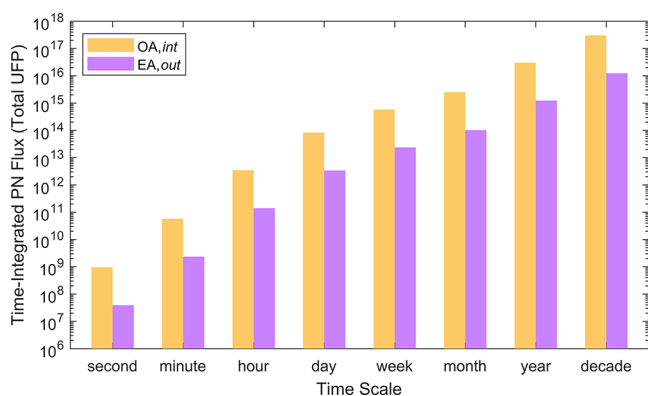


**Figure 10.** Time-integrated UFP transport: total UFP number entering (OA,int; orange) and leaving (EA,out; magenta) an air handling unit, elucidated from 58 days of measurement at the outdoor intake and exhaust, illustrating the magnitude of particle traffic over different time scales, based on a single (20-person capacity) open-plan office with a MERV8 prefilter + HEPA filter in place.

situated on a suburban campus reports a slightly higher median outdoor total PN of  $7.3 \times 10^3$  UFP/cm<sup>3</sup>.<sup>85</sup> In the same study, days experiencing high traffic or pollution incurred PN peaks in the Aitken mode of around  $2.5 \times 10^4$  UFP/cm<sup>3</sup> and accumulation mode averaging  $2 \times 10^4$  UFP/cm<sup>3</sup>.<sup>85</sup> The authors suggest that concentrations below a background of  $4 \times 10^3$  UFP/cm<sup>3</sup> indicate “clean days” absent of strong UFP sources or cleansed by weather for that location,<sup>85</sup> which closely agree with a review identifying a PN of  $3.2 \times 10^3$  UFP/

cm<sup>3</sup> across a survey of studies as a median for “clean” monitoring sites.<sup>86</sup> Another study comparing UFPs at suburban, rural, and urban sites found similar concentrations (peak PN of  $9.4 \times 10^3$  UFP/cm<sup>3</sup>), while also illustrating high rates of new particle formation during the summer paralleling traffic emissions.<sup>87</sup> Although outdoor air PN concentrations can vary by multiple orders of magnitude with a single region,<sup>3</sup> these ranges are congruent with the range of outdoor UFP concentrations reported globally while being lower than sites that are metropolitan or directly roadside, which can reach PN levels as high as  $10^5$  UFP/cm<sup>3</sup> in high-density areas.<sup>3,13,87,88</sup> Previous studies report high PN concentrations emitted from utility plants and airports;<sup>89–92</sup> thus, it is possible that UFPs were sometimes transported from Purdue’s airport and campus utility plant toward the Ray W. Herrick Laboratories. Measured outdoor total PSA concentrations in this campaign, with a median  $PSA_{OA,int}$  of  $140 \mu\text{m}^2/\text{cm}^3$ , closely agree with previously reported PSA concentrations for fine and ultrafine particles ( $10 \text{ nm} \leq D_p \leq 2,500 \text{ nm}$ ), with medians of 120 and  $154 \mu\text{m}^2/\text{cm}^3$  reported for rural<sup>60</sup> and urban<sup>33</sup> environments, respectively. Despite the agreement, PSA UFP measurements remain underreported.

The air handling unit outdoor air intake is regulated by the outdoor air damper position and supply air fan speed, with outdoor air volumetric airflow rates ranging from  $Q_{OA} = 0$  to 4,500 m<sup>3</sup>/h throughout the campaign, ensuring enough outdoor air per occupant. The outdoor air exhibited the highest PN and PSA concentrations within the HVAC system (Figure 4), roughly taking in tens of trillions of UFPs on a daily

basis ( $F_{O_{A,int}} \cdot 24 \text{ h} = 8 \times 10^{13}$  UFPs, Figure 10); however, the outdoor air node has the second highest flux rates illustrated by the PMF, with a median  $F_{O_{A,int}}$  of  $3.5 \times 10^{12}$  UFP/h. The two most notable UFP flux shifts (Figure 5) occur at the mixing of the recirculation and outdoor air yielding the upstream supply air and between the upstream and downstream supply air due to the effects of the prefilter and filter in the air handling unit.

**Supply Air.** Although the recirculation air dilutes the incoming outdoor air to yield lower UFP concentrations, the supply airflow rate is often higher than that in the outdoor air (max  $Q_{SA} = 5 \times 10^3 \text{ m}^3/\text{h}$ ), such as with the day shown in Figure 3. This higher airflow rate in turn contributes to a stronger probability of higher UFP flux rates upstream of the filter bank, with a median  $F_{SA,up}$  of  $4.1 \times 10^{12}$  UFP/h over the sampling summer period when all 4 sensors were present (HEPA period). The downstream supply air flux is at least 1 order of magnitude less than that upstream due to the concentration differential across the HVAC filter bank, with a median  $F_{SA,dn} = 1.7 \times 10^{11}$  UFP/h (HEPA period).

As seen in Table 1, the UFP number and surface area concentrations are slightly higher for the upstream supply air location during the HEPA period (mid-May to November) than during the MERV14 period (mid-February to mid-May). The outdoor air PN concentrations during the MERV14 sampling period—which were not measured—are thus likely lower than those shown for the HEPA period. Replacing the MERV14 filter with a HEPA filter had a noticeable outcome on the downstream supply air PN and PSA concentrations, decreasing from a median  $PN_{SA,dn}$  of 690 UFP/cm<sup>3</sup> to 40 UFP/cm<sup>3</sup> and  $PSA_{SA,dn}$  of  $60 \mu\text{m}^2/\text{cm}^3$  to  $2.5 \mu\text{m}^2/\text{cm}^3$ . Proportionwise, changing to the HEPA filter resulted in a 94% decrease for PN and 97% decrease for PSA, while also reducing the concentration variability of each that persisted through the filter bank. These values are relatively consistent over 3 months (Figure 7). Similar PN concentrations (10 nm  $\leq D_p \leq 1,000$  nm) in the supply air post-HEPA filter have been reported as less than 100 #/cm<sup>3</sup>.<sup>16</sup>

Figure 6 further breaks down the PMFs of UFP fluxes for the supply air locations by filter type (MERV14 or HEPA). The effects of the prefilter were not isolated for in this campaign, but MERV8 has previously been estimated to achieve a median filtration efficiency ranging from 10 to 50% for UFPs greater than 10 nm.<sup>13,93,94</sup> The UFP number-based filtration efficiency of the MERV14 filter, with a  $\eta_{\text{filter}}$  of 40% (25th and 75th percentiles = 30 and 50%) (Figure 6e), resulted in a bimodal postfilter flux PMF (Figure 6a), with a  $F_{SA,dn}$  median of  $1.7 \times 10^{12}$  UFP/h. Figure 7 illustrates the variation in MERV14 efficiency over the 3 monitored months (median PN  $\eta_{\text{filter}} = 33, 48, \text{ and } 41\%$ ; median PSA  $\eta_{\text{filter}} = 27, 34, \text{ and } 30\%$ ), which may be due to time-dependent changes in filter loading and/or particle composition. Using similar methods, Jiang et al. estimated that an energy recovery ventilator running in an air handling unit supplied around  $3.73 \times 10^{11}$  UFP/h to a residence.<sup>4</sup> Switching to a HEPA filter in this campaign reduced the downstream flux an order of magnitude as well as the variability, to a  $F_{SA,dn}$  median of  $1.7 \times 10^{11}$  UFP/h. This reduction implies that roughly a trillion ( $10^{12}$ ) fewer UFPs were supplied to the room each hour, or about tens of trillions ( $10^{13}$ ) daily. The PMFs in Figure 4c and d, including the supply air differential and return air fluxes, further illustrate the stark contrast in the resulting return air when changing the filter from MERV14 to HEPA, from a median  $F_{\text{RetA}}$  of  $1.5 \times 10^{12}$  to  $2.6 \times 10^{11}$  UFP/h. A study using a HEPA-fitted

chamber estimated UFP delivery at background to be around  $10^7$  to  $10^8$  UFP/h,<sup>95</sup> which is intuitively much lower due to stricter source containment and limited infiltration.

The MERV14 efficiency values estimated in this campaign (Figure 6e) fall within the lower end of previously reported values, often ranging 60 to 95% for UFPs from 10 to 100 nm, depending on particle size and face velocity.<sup>13,94</sup> This filtration quality is comparable with deep bag filters shown to be less effective between 5 and 200 nm, with efficiencies varying around 25–50%.<sup>96</sup> In contrast, the median HEPA filtration efficiency was 96% (Figure 4f) throughout the campaign, closely agreeing with previously measured HEPA filters across all particle size ranges.<sup>13</sup> Several of the estimated higher magnitude UFP fluxes in downstream supply air are the result of higher supply air delivery rates (Figure 4b).

Notably, the MERV14 period had relatively similar PN in the downstream supply and return air but less PSA in the return air relative to supply. After changing to HEPA, the PN and PSA show a slight increase in the return air relative to the supply. It is possible that the MERV14 filter allowed higher PSA concentrations to pass through. This provides more sites for coagulation of smaller UFPs and condensation of low-volatility vapors, limiting indoor nucleation and growth events that contribute to UFP total PN detection.<sup>9,97</sup> Thus, this increase in the return air PN during the HEPA period may be explained by the HEPA filter's removal of active particle surface area that would be available as a coagulation or condensation sink, thus allowing for more prolific indoor UFP formation due to the ozonolysis of monoterpenes and skin oil.<sup>98</sup> Because the room was not controlled for occupant activities, it is also likely that there is some seasonal and occupant-based variation. Furthermore, the variation in filtration efficiencies and particles in the downstream supply air may be explained by the composition and concentrations of the particles loading the filter in the upstream supply air.<sup>48</sup>

**Return/Room Air.** Throughout the campaign, notable UFP-generating activities induced by occupants included cleaning by staff or students, using highly volatile odor-control products, eating citrus, and brewing coffee. Because the office does not contain printers or any other high nanoparticle emission appliances that would generate primary aerosols, rapid in-office UFP concentration spikes allude to new particle formation from in-office monoterpene ozonolysis, which has been shown to be readily plausible<sup>99,100</sup> and suggested by episodic fruit-associated monoterpenes measured throughout the campaign.<sup>44</sup>

The living laboratory incurs varying levels of occupancy depending on the day and time of the semester, with occupants spending most of the office time at their desks.<sup>77</sup> Median room UFP concentrations during unoccupied periods during the use of the MERV14 and HEPA filter were  $PN_{\text{RetA}} = 560$  UFP/cm<sup>3</sup> and 80 UFP/cm<sup>3</sup>, respectively, and  $PSA_{\text{RetA}} = 40 \mu\text{m}^2/\text{cm}^3$  and  $4 \mu\text{m}^2/\text{cm}^3$ , respectively. Overall, the median UFP concentrations in the room are  $PN_{\text{RetA}} = 640$  UFP/cm<sup>3</sup> and  $PSA_{\text{RetA}} = 40 \mu\text{m}^2/\text{cm}^3$  during the full MERV14 period, and  $PN_{\text{RetA}} = 100$  UFP/cm<sup>3</sup> and  $PSA_{\text{RetA}} = 3 \mu\text{m}^2/\text{cm}^3$  during the full HEPA period, including both occupied and unoccupied times. Each of these concentrations is well-below the suggested 8-h PN exposure limits of 1,000 UFP/cm<sup>3</sup> for ambient UFPs and 40,000 UFP/cm<sup>3</sup> for workplace nanoparticles.<sup>40,43</sup> Previously reported office UFP concentrations in suburban offices with comparable HVAC filters and lacking high UFP-emitting manufacturing or combustion sources have similarly less than

1,000 UFP/cm<sup>3</sup>,<sup>55</sup> but have also been shown as high as  $3.5 \times 10^4$  in an 80-person HEPA-filtered office with high indoor ozone levels.<sup>16</sup> Background PSA concentrations ( $54 \text{ nm} \leq D_p \leq 565 \text{ nm}$ ) among laboratory and office environments with varying HVAC filters have been reported to average  $10 \mu\text{m}^2/\text{cm}^3$ .<sup>12,101</sup> Other studies report higher UFP concentrations in offices, with PN ranging in medians from  $1.6 \times 10^3$  to  $5.9 \times 10^3$  UFP/cm<sup>3</sup> with varying occupancy levels,<sup>10,24,102</sup> and 500 to  $\sim 1.3 \times 10^3$  UFP/cm<sup>3</sup> in unoccupied offices.<sup>10,24</sup>

Figure 3 illustrates the measured UFP number concentrations, volumetric airflow rates, total office occupancy, and estimated UFP flux rates over the course of 14 h for a select day during the sampling campaign. For this day, the office is occupied by 1–5 people for around 4 h (10 AM–2 PM) before the first noticeable UFP peak of  $5.9 \times 10^3$  UFP/cm<sup>3</sup> from an unknown emission source. The background period in the return air from 6 AM to 8 AM has a UFP flux magnitude of  $F_{\text{RetA}} = 10^{11}$  UFP/h compared to  $10^{13}$  UFP/h during active, occupied hours at the 1:40 PM emission event. The elevated flux of room-sourced particles is also exhausted to the outdoors and recirculated at roughly similar rates ( $F_{\text{RetA}} = 1.4 \times 10^{13}$ ,  $F_{\text{RecrA}} = 8.6 \times 10^{12}$ , and  $F_{\text{EA,out}} = 5.3 \times 10^{12}$  UFP/h, at peak). The recirculated UFPs are then diluted after mixing with the outdoor air at the upstream-filter supply ( $PN_{\text{SA,up}} = 2.7 \times 10^3$  UFP/cm<sup>3</sup>,  $F_{\text{SA,up}} = 6.4 \times 10^{12}$  UFP/h, at the corresponding time) and filtered before re-entering the room supply air gradually at a lower concentration and flux ( $PN_{\text{SA,dn}} = 110$  UFP/cm<sup>3</sup>,  $F_{\text{SA,dn}} = 2.6 \times 10^{11}$  UFP/h). These flux values are similar to size-resolved emission rates estimated for printing-related emissions ( $10^8$  to  $10^{12}$  UFP/h)<sup>22,103</sup> but generally less rapid than cooking-related emission rates from energy-efficient appliances ( $10^{12}$  to  $10^{13}$  UFP/h).<sup>4,104</sup>

Room-specific fluxes (eq 6) elucidated during select known events logged throughout the campaign with noticeable UFP PN peaks can be understood as occupant-sourced emission rates generated at the room node. Median values for these emission rates were grouped into higher and lower categories of magnitude fluxes, resulting in eating citrus fruit (median  $F_{\text{occ}} = 4.3 \times 10^{12}$  UFP/h; 23 events) and brewing coffee, cleaning, and using odor-control products (median  $F_{\text{occ}} = 2.4 \times 10^{11}$  UFP/h; 7 events) (Figure 8). Time-series plots for several observed in-room events revealed that potential UFP-generating activities did not always yield UFP spikes, likely due to factors limiting UFP formation, which is heavily dependent on room conditions including temperature and ozone availability to react with the emitted VOCs.<sup>105,106</sup> The ozone in the office and air handling unit was previously shown to be highly transient,<sup>58</sup> as it is readily depleted in reactions with other airborne VOCs, such as monoterpenes,<sup>18,20,107,108</sup> and skincare products or squalene found on skin and clothes.<sup>16,109,110</sup>

Select observed high emission events are shown in Figure 9, where the PN concentration and flux rates for the return air and pre- and postfilter supply air are plotted temporally over an hour. Figure 9a exemplifies two separate UFP peaks likely arising from ozone-monoterpene reactions, where elevated UFPs are first detected after using an oil diffuser, rising to  $PN_{\text{RetA}}$  of 460 UFP/cm<sup>3</sup> from a background of  $<90$  UFP/cm<sup>3</sup> ( $F_{\text{occ}} = 2.2 \times 10^{11}$  UFP/h), followed by peaking at  $PN_{\text{RetA}}$  of  $4.3 \times 10^3$  UFP/cm<sup>3</sup> from consuming a mandarin ( $F_{\text{occ}} = 2.2 \times 10^{12}$  UFP/h). Figure 9b includes a separate mandarin consumption event, peaking higher at  $PN_{\text{RetA}}$  of  $5.2 \times 10^4$  UFP/cm<sup>3</sup> from a background of  $<60$  UFP/cm<sup>3</sup> ( $F_{\text{occ}} = 1.7 \times$

$10^{13}$  UFP/h). Vartiainen et al. achieved similar magnitudes of 10 nm UFPs peaking around  $2 \times 10^4$  UFP/cm<sup>3</sup>, with emission rates around  $3 \times 10^{12}$  UFP/h.<sup>99</sup> Chamber studies investigating likely similar new particle formation from monoterpene ozonolysis by applying essential oil-based lotion and mosquito repellants have achieved average emission rates of  $1.0 \times 10^9$  UFP/h<sup>17</sup> and ranging  $2.5 \times 10^{10}$  to  $5.9 \times 10^{11}$  UFP/h,<sup>111</sup> respectively, while ensuring the presence of ozone for reactions. The UFP  $PN_{\text{RetA}}$  peak of  $4.0 \times 10^4$  UFP/cm<sup>3</sup> shown in Figure 9c arises from an early morning floor burnishing, with an estimated  $F_{\text{occ}}$  of  $1.4 \times 10^{11}$  UFP/h in a similar range as the indoor ozonolysis events.

**Exhaust and Recirculation Air.** The PMFs in Figure 5b (which includes data solely from the HEPA period) illustrate that return air flux migrates toward recirculation and exhaust air at roughly the same flux rate magnitudes. Because the PN concentrations were assumed to be equal for each of these locations, the shape of each PMF is heavily dependent on the volumetric airflow rates at each location. The recirculation air exhibits a notably bimodal PMF, with median  $F_{\text{RecrA}} = 1.2 \times 10^{11}$  UFP/h. Though the exhaust air PMF is more unimodal, it shares nearly equal flux values, with median  $F_{\text{EA,out}} = 1.1 \times 10^{11}$  UFP/h. These values are each about half of the median return air flux during the HEPA period and are the most likely to have the lowest flux values out of the nodes in the HVAC system at any given time.

The time-integrated fluxes extrapolated from the hourly fluxes in Figure 10 are based on measurements when all four diffusion charger sensors were in position during the HEPA period for 58 complete sampling days. At an hourly rate, 4% ( $\frac{F_{\text{EA,out}}}{F_{\text{OA,int}}}$ ) of the number of UFPs entering the building were exhausted. This proportion is intuitive when considering that the HEPA filter removed 96% of UFPs and accounts for the most notable UFP loss process, indicating that modern office buildings act as a net sink for UFPs. Based on a median hourly outdoor air intake of  $3.5 \times 10^{12}$  UFP/h and exhaust of  $1.1 \times 10^{11}$  UFP/h for this office space, the expected annual UFP intake for this office is estimated to be  $3.0 \times 10^{16}$  UFPs, with an annual UFP exhaust of  $1.2 \times 10^{15}$  UFPs, which would vary based on HVAC filter usage and maintenance. Lower quality filters would allow higher UFP concentrations to be delivered to the room, which would then also be recirculated and exhausted.

The general recommendation for replacing HVAC filters is around 3 months. Using the logic extrapolated for this campaign, a 3-month HEPA filter for this office may collect tens of quadrillions ( $10^{16}$ ) of UFPs, in addition to those of other sizes, with larger particles being filtered out by the MERV8 prefilter. Over a 10-year projected time period, the office would then be expected to intake  $3.0 \times 10^{17}$  UFPs and exhaust  $1.2 \times 10^{16}$  UFPs. The hourly intake and exhaust UFP rates can also be normalized to an office floor area of 104 m<sup>2</sup>, resulting in a  $F_{\text{OA,int}}$  of  $3.3 \times 10^{10}$  UFP/h-m<sup>2</sup> and  $F_{\text{EA,out}}$  of  $1.4 \times 10^9$  UFP/h-m<sup>2</sup>, or a net intake of  $3.2 \times 10^{10}$  UFP/h-m<sup>2</sup>, for this specific 20-person open-plan office.

**Indoor/Outdoor (I/O) Ratios of UFPs on a Number and Surface Area Basis.** The I/O ratios summarized in Figure 4 were estimated for the period when both the indoor and outdoor diffusion charger sensors were present (July to September) by synchronizing the PN or PSA concentrations on a minute basis and then dividing  $P_{\text{RetA}}$  into  $P_{\text{OA,int}}$  at the same minute. Outdoor air measurements were not made

during the MERV14 period. The I/O ratios during the HEPA period sampling time were thus very low, with medians of  $I/O_{PN} = 0.04$  and  $I/O_{PSA} = 0.02$ . These estimated I/O ratios are much lower than those reported in other academic buildings and offices due to higher quality filtration resulting in lower indoor concentrations. Similarly low  $I/O_{PN}$ 's of 0.06 to 0.08 were achieved for particles ranging from 10 to 300 nm using F7 filters ( $\sim$ MERV13),<sup>51</sup> with average indoor PN room concentrations around 250 to 330 UFP/cm<sup>3</sup>.<sup>97</sup>

UFP number size distributions measured while using a MERV8 filter in a commercial rehabilitation center achieved I/O modes of  $I/O_{PN} = 0.15$  for 10–50 nm and 0.1 to 0.3 for 50–100 nm.<sup>11</sup> A similar overall median  $I/O_{PN}$  of 0.17 was achieved for particles less than 500 nm using a glass fiber media filter, rated at an efficiency of 80%,<sup>55</sup> analogous to MERV14 on the basis of UFP removal.<sup>13</sup> Median I/O ratios of 0.20 to 0.38 were achieved using an electrostatic filter among three office buildings containing printers.<sup>96</sup> A higher median of  $I/O_{PN} = 0.5$  was achieved across 10 offices using lower quality filters rated MERV4 to 8.<sup>102</sup> In general, indoor office UFP I/O ratios estimated with PN are noticeably smaller compared to other buildings, especially those with indoor cooking emissions<sup>102</sup> unless there are intense or frequent high emission rate in-room events such as 3D printing.<sup>22,25</sup> The low I/O ratios estimated during this campaign are estimated during a HEPA filter period situated in a high-performance building. This environment is ideal for optimizing IEQ within HVAC operations, which may contrast older buildings that may not have the same resources for higher-energy operation costs and filter maintenance and upkeep.<sup>112</sup>

**Informatics for HVAC Operation and Building Control Integration for Decision-Making.** Number-based flux rates were chosen as a way to model UFP migration within an HVAC system using simultaneous multinodal monitoring pairing diffusion chargers with building automation system data. Mapping these fluxes enables visualization of UFP movement throughout a building, which can be used to evaluate source events and air handling unit performance. It highlights the importance of multipoint UFP detection, as higher particle concentrations may be sourced within the building or from the outdoors, which necessitates different mitigation strategies than for other indoor air pollutants, such as CO<sub>2</sub>. As illustrated, a single or few high-emitting occupant events could cause an in-room PN concentration upward of 10<sup>4</sup> to 10<sup>5</sup> UFP/cm<sup>3</sup> in a brief amount of time by cleaning or eating citrus fruit. Current air handling unit operations centered around demand-based control (e.g., via CO<sub>2</sub> detection) or anticipated demand (temporally programmed supply air delivery) completely overlook aerosol emissions, which are heavily dependent on activity and pre-existing conditions rather than total occupancy. The simplified model used to estimate occupant-sourced flux rates uses a static context-based term ( $\overline{F_{\beta}}$ ) in combination with dynamically measured source and loss terms ( $\overline{F_{RetA}}, \overline{F_{SA,dn}}$ ). Future efforts to monitor a room of concern with high UFP emission rates, such as with printers or combustion, would be able to utilize online UFP sensors upstream and downstream of the room in a similar way to enable real-time flux estimation. This emission rate could either inform the need for source reduction, such as by installing local exhaust hoods, or could be compared with additional sensors enabling outdoor influx rate estimation, for real-time decision-making. Comparing the outdoor influx rate

to indoor emission sources is more imperative in heavily polluted outdoor environments, such as during wildfires, or when using non-HEPA filters, where it cannot be assumed that supplying filtered outdoor air will introduce lower UFP concentrations.

Though UFPs are known to be closely associated with exposure outcomes, there is still a lack of affordable instrumentation that can be used for scalable building integration and automation. There are also no standardized UFP exposure thresholds, though there are time-averaged suggestions based on certain exposures such as nanoparticles as well as suggestions to account for background concentrations to contextualize elevated concentrations.<sup>24,42,43</sup> The challenge of choosing a limit is even more complex when considering particle composition; synthetic and naturally occurring UFPs may follow similar transportation dynamics, while also contributing to different chronic and acute adverse health outcomes.<sup>27</sup> Low-cost optical sensing for PM<sub>2.5</sub> mass concentrations has spurred its widespread usage such that monitoring is available worldwide and can be used by anyone with basic programming skills, as well as integrated within Internet of Things (IoT) frameworks. Further developments in portable aerosol instrumentation capable of detecting UFPs, such as condensation particle counters and diffusion chargers, would similarly allow for wider spread UFP monitoring outside of high-maintenance laboratory environments. Including UFP detection within longitudinal health studies would enable more robust exposure-response scenarios with adverse health effects, providing intel for standard development alongside existing metrics. Lower-cost UFP sensing would also allow for more permanent integration within building systems for UFP-based ventilation control, as well as real-time HVAC assessment for evaluating in-room air cleaning and filtration technologies.

## ■ AUTHOR INFORMATION

### Corresponding Author

**Brandon E. Boor** – Lyles School of Civil & Construction Engineering and Ray W. Herrick Laboratories, Center for High Performance Buildings, Purdue University, West Lafayette, Indiana 47907, United States; [orcid.org/0000-0003-1011-4100](https://orcid.org/0000-0003-1011-4100); Email: [bboor@purdue.edu](mailto:bboor@purdue.edu)

### Authors

**Danielle N. Wagner** – Lyles School of Civil & Construction Engineering and Ray W. Herrick Laboratories, Center for High Performance Buildings, Purdue University, West Lafayette, Indiana 47907, United States

**Nusrat Jung** – Lyles School of Civil & Construction Engineering and Ray W. Herrick Laboratories, Center for High Performance Buildings, Purdue University, West Lafayette, Indiana 47907, United States; [orcid.org/0000-0002-8874-8923](https://orcid.org/0000-0002-8874-8923)

Complete contact information is available at:  
<https://pubs.acs.org/10.1021/acsestair.4c00140>

### Notes

The authors declare no competing financial interest.

## ■ ACKNOWLEDGMENTS

Financial support was provided by the National Science Foundation (CBET-1847493 to B.E.B.) and an American Society of Heating, Refrigerating, and Air Conditioning Engineers Graduate Student Grant-In-Aid Award (to

D.N.W.). The authors would like to thank the staff at the Ray W. Herrick Laboratories for their support in conducting the UFP measurements in the Herrick Living Laboratory office.

## REFERENCES

- (1) Tang, X.; Misztal, P. K.; Nazaroff, W. W.; Goldstein, A. H. Volatile organic compound emissions from humans indoors. *Environ. Sci. Technol.* **2016**, *50* (23), 12686–12694.
- (2) Salma, I.; Dosztály, K.; Borsós, T.; et al. Physical properties, chemical composition, sources, spatial distribution and sinks of indoor aerosol particles in a university lecture hall. *Atmos. Environ.* **2013**, *64*, 219–228.
- (3) Wu, T.; Boor, B. E. Urban aerosol size distributions: A global perspective. *Atmos. Chem. Phys.* **2021**, *21* (11), 8883–8914.
- (4) Jiang, J.; Jung, N.; Boor, B. E. Using Building Energy and Smart Thermostat Data to Evaluate Indoor Ultrafine Particle Source and Loss Processes in a Net-Zero Energy House. *ACS ES&T Eng.* **2021**, *1* (4), 780–793.
- (5) Hussein, T.; Hämeri, K.; Heikkinen, M. S. A.; Kulmala, M. Indoor and outdoor particle size characterization at a family house in Espoo-Finland. *Atmos. Environ.* **2005**, *39* (20), 3697–3709.
- (6) Patel, S.; Sankhyan, S.; Boedicker, E. K.; et al. Indoor Particulate Matter during HOMEChem: Concentrations, Size Distributions, and Exposures. *Environ. Sci. Technol.* **2020**, *54* (12), 7107–7116.
- (7) Shen, G.; Gaddam, C. K.; Ebersviller, S. M.; et al. A Laboratory Comparison of Emission Factors, Number Size Distributions, and Morphology of Ultrafine Particles from 11 Different Household Cookstove-Fuel Systems. *Environ. Sci. Technol.* **2017**, *51* (11), 6522–6532.
- (8) Heitbrink, W. A.; Evans, D. E.; Ku, B. K.; Maynard, A. D.; Slavin, T. J.; Peters, T. M. Relationships among particle number, surface area, and respirable mass concentrations in automotive engine manufacturing. *J. Occup. Environ. Hyg.* **2008**, *6* (1), 19–31.
- (9) Kalaiarasan, G.; Kumar, P.; Tomson, M.; et al. Particle Number Size Distribution in Three Different Microenvironments of London. *Atmosphere* **2024**, *15* (1), 45.
- (10) Cheng, Y. H. Measuring indoor particulate matter concentrations and size distributions at different time periods to identify potential sources in an office building in Taipei City. *Build. Environ.* **2017**, *123*, 446–457.
- (11) Wang, Y.; Hopke, P. K.; Chalupa, D. C.; Utell, M. J. Long-term characterization of indoor and outdoor ultrafine particles at a commercial building. *Environ. Sci. Technol.* **2010**, *44* (15), 5775–5780.
- (12) Niu, J.; Rasmussen, P. E.; Magee, R.; Nilsson, G. Spatial and temporal variability of incidental nanoparticles in indoor workplaces: Impact on the characterization of point source exposures. *Environ. Sci. Technol.* **2015**, *17* (1), 98–109.
- (13) Azimi, P.; Zhao, D.; Stephens, B. Estimates of HVAC filtration efficiency for fine and ultrafine particles of outdoor origin. *Atmos. Environ.* **2014**, *98*, 337–346.
- (14) Vance, M. E.; Marr, L. C. Exposure to airborne engineered nanoparticles in the indoor environment. *Atmos. Environ.* **2015**, *106*, 503–509.
- (15) Manigrasso, M.; Vitali, M.; Protano, C.; Avino, P. Temporal evolution of ultrafine particles and of alveolar deposited surface area from main indoor combustion and non-combustion sources in a model room. *Sci. Total Environ.* **2017**, *598*, 1015–1026.
- (16) Xiang, J.; Weschler, C. J.; Mo, J.; Day, D.; Zhang, J.; Zhang, Y. Ozone, Electrostatic Precipitators, and Particle Number Concentrations: Correlations Observed in a Real Office during Working Hours. *Environ. Sci. Technol.* **2016**, *50* (18), 10236–10244.
- (17) Vannucci, M. P.; Nazaroff, W. W. Ultrafine Particle Production from the Ozonolysis of Personal Care Products. *Environ. Sci. Technol.* **2017**, *51* (21), 12737–12744.
- (18) Stabile, L.; De Luca, G.; Pacitto, A.; Morawska, L.; Avino, P.; Buonanno, G. Ultrafine particle emission from floor cleaning products. *Indoor Air.* **2021**, *31* (1), 63–73.
- (19) Jiang, J.; Ding, X.; Tasoglou, A.; et al. Real-Time Measurements of Botanical Disinfectant Emissions, Transformations, and Multiphase Inhalation Exposures in Buildings. *Environ. Sci. Technol. Lett.* **2021**, *8* (7), 558–566.
- (20) Rosales, C. M. F.; Jiang, J.; Lahib, A.; et al. Chemistry and human exposure implications of secondary organic aerosol production from indoor terpene ozonolysis. *Sci. Adv.* **2022**, *8* (8), 1–16.
- (21) Salthammer, T.; Schripp, T.; Uhde, E.; Wensing, M. Aerosols generated by hardcopy devices and other electrical appliances. *Environ. Pollut.* **2012**, *169*, 167–174.
- (22) Dunn, K. L.; Hammond, D.; Menchaca, K.; Roth, G.; Dunn, K. H. Reducing ultrafine particulate emission from multiple 3D printers in an office environment using a prototype engineering control. *J. Nanoparticle Res.* **2020**, *22* (5), 1–11.
- (23) Tang, T.; Hurraß, J.; Gminski, R.; Mersch-Sundermann, V. Fine and ultrafine particles emitted from laser printers as indoor air contaminants in German offices. *Environ. Sci. Pollut. Res.* **2012**, *19* (9), 3840–3849.
- (24) McGarry, P.; Morawska, L.; He, C.; et al. Exposure to particles from laser printers operating within office workplaces. *Environ. Sci. Technol.* **2011**, *45* (15), 6444–6452.
- (25) Viitanen, A.-K.; Kallonen, K.; Kukko, K.; Kanerva, T.; Saukko, E.; Hussein, T.; Hämeri, K.; Saamanen, A. Technical control of nanoparticle emissions from desktop 3D printing. *Indoor Air* **2021**, *31* (4), 1061–1071.
- (26) Liu, N. M.; Miyashita, L.; Maher, B. A.; et al. Evidence for the presence of air pollution nanoparticles in placental tissue cells. *Sci. Total Environ.* **2021**, *751*, No. 142235.
- (27) Oberdörster, G.; Oberdörster, E.; Oberdörster, J. Nanotoxicology: An emerging discipline evolving from studies of ultrafine particles. *Environ. Health Perspect.* **2005**, *113* (7), 823–839.
- (28) Xia, T.; Korge, P.; Weiss, J. N.; et al. Quinones and aromatic chemical compounds in particulate matter induce mitochondrial dysfunction: Implications for ultrafine particle toxicity. *Environ. Health Perspect.* **2004**, *112* (14), 1347–1358.
- (29) Schraufnagel, D. E. The health effects of ultrafine particles. *Exp. Mol. Med.* **2020**, *52* (3), 311–317.
- (30) Tyler, C. R.; Zychowski, K. E.; Sanchez, B. N.; et al. Surface area-dependence of gas-particle interactions influences pulmonary and neuroinflammatory outcomes. *Part. Fibre Toxicol.* **2016**, *13* (1), 1–18.
- (31) Elder, A.; Gelein, R.; Silva, V.; et al. Translocation of inhaled ultrafine manganese oxide particles to the central nervous system. *Environ. Health Perspect.* **2006**, *114* (8), 1172–1178.
- (32) Jiang, Y.; Zhu, X.; Shen, Y.; et al. Mechanistic insights into cardiovascular effects of ultrafine particle exposure: A longitudinal panel study. *Environ. Int.* **2024**, *187* (May), No. 108714.
- (33) Lin, S.; Ryan, I.; Paul, S.; et al. Particle surface area, ultrafine particle number concentration, and cardiovascular hospitalizations. *Environ. Pollut.* **2022**, *310*, No. 119795.
- (34) Jew, K.; Herr, D.; Wong, C.; et al. Selective memory and behavioral alterations after ambient ultrafine particulate matter exposure in aged 3xTgAD Alzheimer's disease mice. *Part. Fibre Toxicol.* **2019**, *16* (1), 1–17.
- (35) Cory-Slechta, D. A.; Allen, J. L.; Conrad, K.; Marvin, E.; Sobolewski, M. Developmental Exposure to Low Level Ambient Ultrafine Particle Air Pollution and Cognitive Dysfunction. *Neurotoxicology* **2018**, *69* (5), 217–231.
- (36) Ogurtsova, K.; Soppa, V. J.; Weimar, C.; Jöckel, K. H.; Jokisch, M.; Hoffmann, B. Association of long-term air pollution and ambient noise with cognitive decline in the heinz nixdorf recall study. *Environ. Pollut.* **2023**, *331*, No. 121898.
- (37) Patten, K. T.; Valenzuela, A. E.; Wallis, C.; et al. The effects of chronic exposure to ambient traffic-related air pollution on Alzheimer's disease phenotypes in wildtype and genetically predisposed male and female rats. *Environ. Health Perspect.* **2021**, *129* (5), 1–14.
- (38) Schmid, O.; Stoeger, T. Surface area is the biologically most effective dose metric for acute nanoparticle toxicity in the lung. *J. Aerosol Sci.* **2016**, *99*, 133–143.

- (39) Cassee, F. R.; Héroux, M. E.; Gerlofs-Nijland, M. E.; Kelly, F. J. Particulate matter beyond mass: Recent health evidence on the role of fractions, chemical constituents and sources of emission. *Inhal. Toxicol.* **2013**, *25* (14), 802–812.
- (40) WHO *Global Air Quality Guidelines: Particulate Matter (PM<sub>2.5</sub> and PM<sub>10</sub>), Ozone, Nitrogen Dioxide, Sulfur Dioxide and Carbon Monoxide: Executive Summary*; World Health Organization, 2021. <https://iris.who.int/handle/10665/345334> (accessed September 16, 2024).
- (41) Stoeger, T.; Reinhard, C.; Takenaka, S.; et al. Instillation of six different ultrafine carbon particles indicates a surface area threshold dose for acute lung inflammation in mice. *Environ. Health Perspect.* **2006**, *114* (3), 328–333.
- (42) Visser, M.; Gosens, I.; Bard, D.; et al. Towards health-based nano reference values (HNRVs) for occupational exposure: Recommendations from an expert panel. *NanoImpact.* **2022**, *26*, No. 100396.
- (43) *Provisional Nano Reference Values for Engineered Nanomaterials*; Advisory Report 12/01; Sociaal-Economische Raad: Den Haag, The Netherlands, 2012. <https://www.ser.nl/-/media/ser/downloads/adviezen/2012/voorlopige-nanoreferentievoorwaarden.pdf> (accessed September 16, 2024).
- (44) Wu, T.; Tasoglou, A.; Wagner, D. N.; et al. Modern Buildings Act as a Dynamic Source and Sink for Urban Air Pollutants. *Cell Rep. Sustain.* **2024**, *1* (5), No. 100103.
- (45) *Energy and Emissions Building Performance Standard for Existing Buildings*; ANSI/ASHRAE/IES 100-2024; ANSI/ASHRAE: Peachtree Corners, GA, 2024.
- (46) *Method of Testing General Ventilation Air-Cleaning Devices for Removal Efficiency by Particle Size*; ANSI/ASHRAE 52.2-2017; ANSI/ASHRAE: Atlanta, GA, 2017.
- (47) *Ventilation and Acceptable Indoor Air Quality*; ANSI/ASHRAE 62.1-2022; ANSI/ASHRAE: Peachtree Corners, GA, 2022.
- (48) Ardkapan, S. R.; Johnson, M. S.; Yazdi, S.; Afshari, A.; Bergsøe, N. C. Filtration efficiency of an electrostatic fibrous filter: Studying filtration dependency on ultrafine particle exposure and composition. *J. Aerosol Sci.* **2014**, *72*, 14–20.
- (49) Hecker, R.; Hofacre, K. C.; Wood, J.; Sparks, L. *Final Report on Development of Performance Data for Common Building Air Cleaning Devices*; U.S. Environmental Protection Agency, Office of Research and Development, National Homeland Security Research Center, Decontamination and Consequence Management, 2008.
- (50) Li, T.; Siegel, J. A. In situ efficiency of filters in residential central HVAC systems. *Indoor Air.* **2020**, *30* (2), 315–325.
- (51) Shi, B.; Ekberg, L. E.; Langer, S. Intermediate air filters for general ventilation applications: An experimental evaluation of various filtration efficiency expressions. *Aerosol Sci. Technol.* **2013**, *47* (5), 488–498.
- (52) Leavey, A.; Fu, Y.; Sha, M.; et al. Air quality metrics and wireless technology to maximize the energy efficiency of HVAC in a working auditorium. *Build. Environ.* **2015**, *85*, 287–297.
- (53) Patra, S. S.; Ramsisaria, R.; Du, R.; Wu, T.; Boor, B. E. A machine learning field calibration method for improving the performance of low-cost particle sensors. *Build. Environ.* **2021**, *190*, No. 107457.
- (54) Pelliccioni, A.; Gherardi, M. Development and validation of an intra-calibration procedure for MiniDISCs measuring ultrafine particles in multi-spatial indoor environments. *Atmos. Environ.* **2021**, *246*, No. 118154.
- (55) Chatoutsidou, S. E.; Ondráček, J.; Tesar, O.; Tørseth, K.; Ždímal, V.; Lazaridis, M. Indoor/outdoor particulate matter number and mass concentration in modern offices. *Build. Environ.* **2015**, *92*, 462–474.
- (56) Silvonon, V.; Salo, L.; Raunima, T.; Vojtisek-Lom, M.; Ondracek, J.; Topinka, J.; Schins, R. P.F.; Lepisto, T.; Lintusaari, H.; Saarikoski, S.; Barreira, L. M.F.; Hoivala, J.; Markkula, L.; Kulmala, I.; Vinha, J.; Karjalainen, P.; Ronkko, T. Lung-depositing surface area (LDSA) of particles in office spaces around Europe: Size distributions, I/O-ratios and infiltration. *Build. Environ.* **2023**, *246*, No. 110999.
- (57) Stephens, B.; Siegel, J. A. Ultrafine particle removal by residential heating, ventilating, and air-conditioning filters. *Indoor Air.* **2013**, *23* (6), 488–497.
- (58) Jiang, J.; Wu, T.; Wagner, D. N.; et al. Investigating how occupancy and ventilation mode influence the dynamics of indoor air pollutants in an office environment. *ASHRAE Trans.* **2020**, *126*, 464–473.
- (59) Fazli, T.; Zeng, Y.; Stephens, B. Fine and ultrafine particle removal efficiency of new residential HVAC filters. *Indoor Air.* **2019**, *29* (4), 656–669.
- (60) Wagner, D. N.; Odhiambo, S. R.; Ayikukwei, R. M.; Boor, B. E. High time-resolution measurements of ultrafine and fine woodsmoke aerosol number and surface area concentrations in biomass burning kitchens: A case study in Western Kenya. *Indoor Air.* **2022**, *32* (10), e13132.
- (61) Matson, U. Indoor and outdoor concentrations of ultrafine particles in some Scandinavian rural and urban areas. *Sci. Total Environ.* **2005**, *343* (1–3), 169–176.
- (62) Li, J.; Li, H.; Ma, Y.; Wang, Y.; Abokifa, A. A.; Lu, C.; Biswas, P. Spatiotemporal distribution of indoor particulate matter concentration with a low-cost sensor network. *Build. Environ.* **2018**, *127*, 138–147.
- (63) Demanega, I.; Mujan, I.; Singer, B. C.; Anđelković, A. S.; Babich, F.; Licina, D. Performance assessment of low-cost environmental monitors and single sensors under variable indoor air quality and thermal conditions. *Build. Environ.* **2021**, *187*, No. 107415.
- (64) Ben-David, T.; Wang, S.; Rakes, A.; Waring, M. S. Measuring the efficacy of HVAC particle filtration over a range of ventilation rates in an office building. *Build. Environ.* **2018**, *144*, 648–656.
- (65) Patel, S.; Li, J.; Pandey, A.; Pervez, S.; Chakrabarty, R. K.; Biswas, P. Spatio-temporal measurement of indoor particulate matter concentrations using a wireless network of low-cost sensors in households using solid fuels. *Environ. Res.* **2017**, *152*, 59–65.
- (66) Tsameret, S.; Furuta, D.; Saha, P.; et al. Low-Cost Indoor Sensor Deployment for Predicting PM<sub>2.5</sub> Exposure. *ACS EST Air* **2024**, *1* (8), 767–779.
- (67) Burkart, J.; Steiner, G.; Reischl, G.; Moshhammer, H.; Neuberger, M.; Hitzemberger, R. Characterizing the performance of two optical particle counters (Grimm OPC1.108 and OPC1.109) under urban aerosol conditions. *J. Aerosol Sci.* **2010**, *41* (10), 953–962.
- (68) Li, J.; Mattewal, S. K.; Patel, S.; Biswas, P. Evaluation of nine low-cost-sensor-based particulate matter monitors. *Aerosol Air Qual. Res.* **2020**, *20* (2), 254–270.
- (69) Welker, R. W. *Size Analysis and Identification of Particles*, Vol. 4; Elsevier, 2012.
- (70) Asbach, C.; Schmitz, A.; Schmidt, F.; Monz, C.; Todea, A. M. Intercomparison of a personal CPC and different conventional CPCs. *Aerosol Air Qual. Res.* **2017**, *17* (5), 1132–1141.
- (71) Mordas, G.; Manninen, H. E.; Petējā, T.; Aalto, P. P.; Hämeri, K.; Kulmala, M. On operation of the ultra-fine water-based CPC TSI 3786 and comparison with other TSI models (TSI 3776, TSI 3772, TSI 3025, TSI 3010, TSI 3007). *Aerosol Sci. Technol.* **2008**, *42* (2), 152–158.
- (72) Szigeti, T.; Dunster, C.; Cattaneo, A.; et al. Spatial and temporal variation of particulate matter characteristics within office buildings — The OFFICAIR study. *Sci. Total Environ.* **2017**, *587–588*, 59–67.
- (73) Maricq, M. M. Monitoring Motor vehicle PM emissions: An evaluation of three portable low-cost aerosol instruments. *Aerosol Sci. Technol.* **2013**, *47* (5), 564–573.
- (74) Kaminski, H.; Kuhlbusch, T. A. J.; Rath, S.; et al. Comparability of mobility particle sizers and diffusion chargers. *J. Aerosol Sci.* **2013**, *57*, 156–178.
- (75) Lee, S.; Joe, J.; Karava, P.; Bilonis, I.; Tzempelikos, A. Implementation of a self-tuned HVAC controller to satisfy occupant

- thermal preferences and optimize energy use. *Energy Build.* **2019**, *194*, 301–316.
- (76) Joe, J.; Karava, P. A model predictive control strategy to optimize the performance of radiant floor heating and cooling systems in office buildings. *Appl. Energy.* **2019**, *245*, 65–77.
- (77) Wagner, D. N.; Mathur, A.; Boor, B. E. Spatial seated occupancy detection in offices with a chair-based temperature sensor array. *Build. Environ.* **2021**, *187*, No. 107360.
- (78) Lu, Y.; Huang, J.; Wagner, D. N.; Lin, Z.; Jung, N.; Boor, B. E. The influence of displacement ventilation on indoor carbon dioxide exposure and ventilation efficiency in a living laboratory open-plan office. *Build. Environ.* **2024**, *256*, No. 111468.
- (79) Patra, S. S.; Wu, T.; Wagner, D. N.; Jiang, J.; Boor, B. E. Real-time measurements of fluorescent aerosol particles in a living laboratory office under variable human occupancy and ventilation conditions. *Build. Environ.* **2021**, *205*, No. 108249.
- (80) Wu, T.; Boor, B. E. Characterization of a thermal aerosol generator for HVAC filtration experiments (RP-1734). *Sci. Technol. Built Environ.* **2020**, *26* (6), 816–834.
- (81) Sippola, M. R.; Nazaroff, W. W. Modeling particle loss in ventilation ducts. *Atmos. Environ.* **2003**, *37* (39–40), 5597–5609.
- (82) Miller, S. L.; Facciola, N. A.; Toohey, D.; Zhai, J. Ultrafine and fine particulate matter inside and outside of mechanically ventilated buildings. *Int. J. Environ. Res. Public Health.* **2017**, *14* (2), 128.
- (83) Thatcher, T. L.; Lai, A. C. K.; Moreno-Jackson, R.; Sextro, R. G.; Nazaroff, W. W. Effects of room furnishings and air speed on particle deposition rates indoors. *Atmos. Environ.* **2002**, *36* (11), 1811–1819.
- (84) Wallace, L. Indoor Particles: A Review. *J. Air Waste Manage. Assoc.* **1996**, *46* (2), 98–126.
- (85) Rímnáková, D.; Ždímal, V.; Schwarz, J.; Smolík, J.; Rímnác, M. Atmospheric aerosols in suburb of Prague: The dynamics of particle size distributions. *Atmos. Res.* **2011**, *101* (3), 539–552.
- (86) Morawska, L.; Ristovski, Z.; Jayaratne, E. R.; Keogh, D. U.; Ling, X. Ambient nano and ultrafine particles from motor vehicle emissions: Characteristics, ambient processing and implications on human exposure. *Atmos. Environ.* **2008**, *42* (35), 8113–8138.
- (87) Gani, S.; Chambliss, S. E.; Messier, K. P.; Lunden, M. M.; Apte, J. S. Spatiotemporal profiles of ultrafine particles differ from other traffic-related air pollutants: Lessons from long-term measurements at fixed sites and mobile monitoring. *Environ. Sci.: Atmos.* **2021**, *1* (7), 558–568.
- (88) Kumar, P.; Morawska, L.; Birmili, W.; Paasonen, P.; Hu, M.; Kulmala, M.; Harrison, R. M.; Norford, L.; Britter, R. Ultrafine particles in cities. *Environ. Int.* **2014**, *66*, 1–10.
- (89) Bond, T. C.; Wehner, B.; Plewka, A.; Wiedensohler, A.; Heintzenberg, J.; Charlson, R. J. Climate-relevant properties of primary particulate emissions from oil and natural gas combustion. *Atmos. Environ.* **2006**, *40* (19), 3574–3587.
- (90) Zimmerman, A.; Petters, M. D.; Meskhidze, N. Observations of new particle formation, modal growth rates, and direct emissions of sub-10 nm particles in an urban environment. *Atmos. Environ.* **2020**, *242*, No. 117835.
- (91) Lawal, A. S.; Russell, A. G.; Kaiser, J. Assessment of Airport-Related Emissions and Their Impact on Air Quality in Atlanta, GA, Using CMAQ and TROPOMI. *Environ. Sci. Technol.* **2022**, *56* (1), 98–108.
- (92) Stacey, B.; Harrison, R. M.; Pope, F. D. Emissions of ultrafine particles from civil aircraft: dependence upon aircraft type and passenger load. *NPJ Clim. Atmos. Sci.* **2023**, *6* (1), 1–9.
- (93) Alavy, M.; Siegel, J. A. In-situ effectiveness of residential HVAC filters. *Indoor Air.* **2020**, *30* (1), 156–166.
- (94) Brochot, C.; Abdolghader, P.; Haghghat, F.; Bahloul, A. Performance of mechanical filters used in general ventilation against nanoparticles. *Sci. Technol. Built Environ.* **2020**, *26* (10), 1387–1396.
- (95) Koivisto, A. J.; Hussein, T.; Niemelä, R.; Tuomi, T.; Hämeri, K. Impact of particle emissions of new laser printers on modeled office room. *Atmos. Environ.* **2010**, *44* (17), 2140–2146.
- (96) Quang, T. N.; He, C.; Morawska, L.; Knibbs, L. D. Influence of ventilation and filtration on indoor particle concentrations in urban office buildings. *Atmos. Environ.* **2013**, *79*, 41–52.
- (97) Orru, H.; Hagenbjörk, A.; Olstrup, H. Indoor and outdoor nanoparticle concentrations in an urban background area in northern Sweden: The nanooffice study. *Environments.* **2021**, *8* (8), 75.
- (98) Patra, S. S.; Jiang, J.; Ding, X.; et al. Dynamics of nanocluster aerosol in the indoor atmosphere during gas cooking. *PNAS Nexus.* **2024**, *3* (2), pgae044.
- (99) Vartiainen, E.; Kulmala, M.; Ruuskanen, T. M.; Taipale, R.; Rinne, J.; Vehkamäki, H. Formation and growth of indoor air aerosol particles as a result of d-limonene oxidation. *Atmos. Environ.* **2006**, *40* (40), 7882–7892.
- (100) Langer, S.; Moldanová, J.; Arrhenius, K.; Ljungström, E.; Ekberg, L. Ultrafine particles produced by ozone/limonene reactions in indoor air under low/closed ventilation conditions. *Atmos. Environ.* **2008**, *42* (18), 4149–4159.
- (101) Vosburgh, D. J. H.; Ku, B. K.; Peters, T. M. Evaluation of a diffusion charger for measuring aerosols in a workplace. *Ann. Occup. Hyg.* **2014**, *58* (4), 424–436.
- (102) Wu, X.; Apte, M. G.; Bennett, D. H. Indoor particle levels in small- and medium-sized commercial buildings in California. *Environ. Sci. Technol.* **2012**, *46* (22), 12355–12363.
- (103) He, C.; Morawska, L.; Taplin, L. Particle Emission Characteristics of Office Printers. *Environ. Sci. Technol.* **2007**, *41* (17), 6039–6045.
- (104) Rim, D.; Choi, J. I.; Wallace, L. A. Size-Resolved Source Emission Rates of Indoor Ultrafine Particles Considering Coagulation. *Environ. Sci. Technol.* **2016**, *50* (18), 10031–10038.
- (105) Nørgaard, A. W.; Kudal, J. D.; Kofoed-Sørensen, V.; Koponen, I. K.; Wolkoff, P. Ozone-initiated VOC and particle emissions from a cleaning agent and an air freshener: Risk assessment of acute airway effects. *Environ. Int.* **2014**, *68*, 209–218.
- (106) Chen, J.; Möller, K. H.; Wennberg, P. O.; Kjaergaard, H. G. Unimolecular Reactions following Indoor and Outdoor Limonene Ozonolysis. *J. Phys. Chem. A* **2021**, *125* (2), 669–680.
- (107) Youssefi, S.; Waring, M. S. Indoor transient SOA formation from ozone+ $\alpha$ -pinene reactions: Impacts of air exchange and initial product concentrations, and comparison to limonene ozonolysis. *Atmos. Environ.* **2015**, *112*, 106–115.
- (108) Coleman, B. K.; Lunden, M. M.; Destailats, H.; Nazaroff, W. W. Secondary organic aerosol from ozone-initiated reactions with terpene-rich household products. *Atmos. Environ.* **2008**, *42* (35), 8234–8245.
- (109) Lakey, P. S. J.; Morrison, G. C.; Won, Y.; et al. The impact of clothing on ozone and squalene ozonolysis products in indoor environments. *Commun. Chem.* **2019**, *2* (1), 2–9.
- (110) Wang, N.; Müller, T.; Ernle, L.; Bekö, G.; Wargocki, P.; Williams, J. How Does Personal Hygiene Influence Indoor Air Quality? *Environ. Sci. Technol.* **2024**, *58* (22), 9750–9759.
- (111) Liu, J.; Fung, D.; Jiang, J.; Zhu, Y. Ultrafine particle emissions from essential-oil-based mosquito repellent products. *Indoor Air.* **2014**, *24* (3), 327–335.
- (112) Zhang, Y.; Hui, F. K. P.; Duffield, C.; Saeed, A. M. A review of facilities management interventions to mitigate respiratory infections in existing buildings. *Build. Environ.* **2022**, *221* (March), No. 109347.